SUPPLEMENTAL MATERIAL

Local Peroxynitrite Impairs Endothelial TRPV4 Channels and Elevates Blood Pressure in Obesity

Matteo Ottolini, M.S.[†1,2]; Kwangseok Hong, Ph.D.[†1]; Eric L. Cope, B.S.[1]; Zdravka Daneva, Ph.D.[1]; Leon J. DeLalio, Ph.D.[1]; Jennifer D. Sokolowski, M.D. Ph.D[3]; Corina Marziano, Ph.D.[1,4]; Nhiem Y. Nguyen, B.S.[1]; Joachim Altschmied, Ph.D.[5]; Judith Haendeler, Ph.D.[5,6]; Scott R. Johnstone, PhD.[1], Mohammad Y. Kalani, M.D. Ph.D.[3], Min S. Park, M.D.[3], Rakesh P. Patel, Ph.D.[7], Wolfgang Liedtke, M.D., Ph.D.[8]; Brant E. Isakson, Ph.D.[1,4]; and Swapnil K. Sonkusare, Ph.D.[1,2,4]*

[1]Robert M. Berne Cardiovascular Research Center, University of Virginia-School of Medicine, Charlottesville, VA, 22908, USA; [2]Department of Pharmacology, University of Virginia-School of Medicine, Charlottesville, VA, 22908, USA; [3]Department of Neurological Surgery, University of Virginia, Charlottesville, VA, 22908, USA; [4]Department of Molecular Physiology and Biological Physics, University of Virginia-School of Medicine, Charlottesville, VA, 22908, USA; [5]IUF-Leibniz Research Institute for Environmental Medicine, Duesseldorf, 40021, Germany; [6] Institute of Clinical Chemistry and Laboratory Diagnostic, Medical Faculty, University of Duesseldorf, Duesseldorf, 40021, Germany; [7]Department of Pathology and Center for Free Radical Biology, University of Alabama at Birmingham, Birmingham, AL, 35294, USA; [8]Department of Neurology, Duke University School of Medicine, Durham, NC, 27710, USA

[†]Authors contributed equally

Running Title: Peroxynitrite inhibits TRPV4 channel function in obesity

***Correspondence should be addressed to:**

Swapnil K. Sonkusare, Ph.D.

Room 6051A, Medical Research Building 4 (MR4), 409 Lane Rd

University of Virginia-School of Medicine, Charlottesville VA 22908

E-mail: sks2n@virginia.edu

Phone: 434-297-7401

SUPPLEMENTAL METHODS

Animal Protocols. All animal protocols were approved by the University of Virginia Animal Care and Use Committee (Protocols 4120 and 4051). A total of 210 mice were used in the study. Male C57BL6/J with normal chow (normal fat diet or NFD: 10% kcal fat) or high-fat diet (HFD: 60% kcal fat, Research Diets Inc., New Brunswick, NJ, USA; 14 weeks starting at 6 weeks of age), and endothelium-specific TRPV4 ($TRPV4_{EC}^{-/-}$) and AKAP150 ($AKAP150_{EC}^{-/-}$) knockout mice (12-14 weeks old) were used in the present study. Female C57BL6/J mice fed a high-fat diet for 14 weeks did not show endothelial dysfunction, therefore, only male mice were used in this study. Some of $TRPV4_{EC}^{-/-}$ mice were fed HFD for 14 weeks. Mice were euthanized with pentobarbital (90 mg/kg, intraperitoneal) followed by decapitation for harvesting gut tissues. Third-order mesenteric arteries (MAs, ~100 μm) were dissected in cold Hepes-buffered physiological salt solution (Hepes-PSS; 10 mM Hepes, 134 mM NaCl, 6 mM KCl, 1 mM $MgCl_2$ hexahydrate, 2 mM $CaCl_2$ dihydrate, and 7 mM dextrose, pH adjusted to 7.4 using 1M NaOH). The perivascular adipose tissue was removed for all the *ex vivo* experiments.

For *in vivo* experiments, an independent team member performed random assignment of animals to groups and did not have knowledge of treatment assignment groups. All the *in vivo* experiments were blinded; information about the groups or treatments was withheld from the experimenter or from the team member who analyzed the data. All the experiments were performed in at least two independent batches.

Isolation of human splenius and temporalis muscle tissue. Splenius and temporalis muscle tissue were obtained from non-obese (BMI ≤ 25) and obese (BMI ≥ 30) individuals during craniotomy surgeries as approved by University of Virginia Institutional Review Board (Protocol # 18699). Informed consents were obtained as per the protocol. Small arteries (~ 100 μm) were dissected out from the muscle tissue in cold Hepes-PSS. Samples from 8 individuals were used in the study (4 non-obese and 4 obese).

Generation of $TRPV4_{EC}^{-/-}$ and $AKAP150_{EC}^{-/-}$ mice. $TRPV4_{EC}^{-/-}$ or $AKAP150_{EC}^{-/-}$ mice were generated by crossing $TRPV4^{lox/lox}$ [1] or $AKAP150^{lox/lox}$ (The Jackson Laboratory, Bar Harbor, ME, USA) mice with tamoxifen-inducible VE-Cadherin (Cdh5) Cre mice[2]. $AKAP150^{lox/lox}$ Cre^{+} or $TRPV4^{lox/lox}$ Cre^{+} mice were injected with tamoxifen (Sigma-Aldrich, St. Louis, MO, USA) at 6 weeks of age (40 mg/kg i.p. per day for 10 days), followed by a 2-week washout period. $AKAP150^{lox/lox}$ Cre^{-} or $TRPV4^{lox/lox}$ Cre^{-} mice injected with tamoxifen were used as Wild-type (WT) control mice. Immunostaining for $TRPV4_{EC}$ or $AKAP150_{EC}$ or endothelial cell mRNA levels for $TRPV4_{EC}$ or $AKAP150_{EC}$ (described below) were compared to confirm endothelial knockout of TRPV4 or AKAP150.

Genotyping. Samples of ear tissue were treated with the HotSHOT lysis buffer (25 mM NaOH, 0.2 mM EDTA) and neutralized with an equal volume 40 mM Tris-HCL to extract genomic DNA. Polymerase Chain Reactions were performed using 1 unit Bioline MangoTaq Polymerase and buffer (London, England), 1.5 mM $MgCl_2$, 200 μM of each dNTP, 1 μM 5' and 3' primers, and approximately 100-250 ng genomic DNA, and run on a Bio-Rad T100 Thermal Cycler (Hercules, CA). Reaction products were then run on a 1% agarose gel containing 0.2 μg/μL ethidium bromide in TAE Buffer (40 mM Tris Base, 20 mM Acetic Acid, 1 mM EDTA) at 90V

using a Bio-Rad PowerPac HC High-Current Power Supply. Gels were visualized by exposing to 302 nm UV light and compared to a New England BioLabs 100 bp DNA Ladder (Ipswich, MA). The genotyping primers included: Cdh5 Cre, 5' GCCTGCATTACCGGTCGATGCAACGA, 3' GTGGCAGATGGCGCGGCAACACCATT; TRPV4^{loxP}, 5' CATGAAATCTGACCTCTTGTCCCC, 3' TTGTGTACTGTCTGCACACCAGGC; AKAP150^{loxP}, 5' GAAAGTAGCGCCTCCTTGGT, 3' TGCTCAGATTTTGTTTGAGGTC. All primers were ordered from Eurofins Genomics (Louisville, KY).

Pressure myography. Third-order MAs from mice or human splenius/temporalis muscle arteries were cannulated onto two glass micropipettes on a custom-made pressure myography chamber (The Instrumentation and Model Facility, University of Vermont, Burlington, VT, USA), and pressurized to 80 mmHg with a pressure servo controller peristaltic pump (Living Systems Instrumentation, St Albans, VT, USA). The vessels were superfused with PSS (119 mM NaCl, 4.7 mM KCl, 1.2 mM KH_2PO4, 1.2 mM $MgCl_2$ 160 hexahydrate, 2.5 mM $CaCl_2$ dihydrate, 7 mM dextrose, and 24 mM $NaHCO_3$) at 37 °C, and bubbled with 21% O_2 and 5% CO_2 to maintain the pH at 7.4. Mouse arteries were allowed to develop spontaneous pressure-induced constriction (myogenic tone) at 80 mmHg before the start of experimental treatment; human arteries were pre-constricted with U46619 (thromboxane A2 receptor agonist, 50 nM). Dilation to NS309 (1 μM), a direct opener of intermediate/small conductance Ca^{2+} -sensitive K^+ (IK/SK) channels, was used to functionally assess endothelial cells health. Arteries that failed to show a maximal dilation to NS309 were discarded. Pharmacological agents were applied directly to the PSS superfusion and were incubated for 5 −10-min. For the experiments using 60 mM K^+ PSS, the arteries were superfused with 60 mM K^+-containing PSS (in mM, 64.9 NaCl, 58.8 KCl, 1.2 KH_2PO_4, 1.2 $MgCl_2$, 7 glucose, 24 $NaHCO_3$, 2 $CaCl_2$). At the end of each experiment, the arteries were incubated with Ca^{2+}-free PSS solution (119 mM NaCl, 4.7 mM KCl,1.2 mM KH_2PO_4,1.2 mM $MgCl_2$, 7 mM glucose, 24 mM $NaHCO_3$, 5 mM EGTA (pH 7.4)) to evaluate the maximum passive diameter. Internal diameter was recorded at 10 frames/second using a CCD (charged-coupled device) camera and analyzed using IonOptix edge detection software (IonOptix LLC, Westwood, MA USA). Myogenic vasoconstriction at 80 mm Hg was calculated as:

$$\left[\frac{\left(Diameter_{Ca\ free} - Diameter_{constricted}\right)}{Diameter_{Ca\ free}}\right] * 100$$

where $Diameter_{constricted}$ is the diameter of the artery after generating myogenic vasoconstriction, and $Diameter_{Ca\ free}$ is the maximum passive diameter.

Percent vasodilation was calculated by:

$$\left[\frac{(Diameter_{dilated} - Diameter_{basal})}{(Diameter_{Ca\ free} - Diameter_{basal})}\right] * 100$$

Where $Diameter_{basal}$ is the diameter before adding the drug, $Diameter_{dilated}$is the diameter after adding the drug and $Diameter_{Ca\ free}$ is the maximum passive diameter.

Radiotelemetric blood pressure measurement. Continuous blood pressure measurements were performed using Dataquest A.R.T. 20 software (Data Sciences International, St. Paul, MN), as described previously[3, 4]. AKAP150$_{EC}^{-/-}$, TRPV4$_{EC}^{-/-}$, and respective WT mice, NFD and HFD mice were anesthetized with isoflurane (1.5%) and radiotelemetry catheter (TA11PA-C10, Data Sciences International, St. Paul, MN) was implanted in the left carotid artery. The catheter was tunneled through to the radiotransmitter, which was placed in a subcutaneous pouch along the flank. Before arterial pressure measurements were initiated, mice were allowed to recover for seven days after surgery to regain normal circadian rhythms. Baseline systolic, diastolic, and mean arterial pressures, and heart rate were recorded continuously over 72 hours (at 1-min intervals) following the recovery period. The values over three days (6 AM to 6 PM) and three nights (6 PM to 6 AM) were averaged to obtain the baseline day- or night-time blood pressures and heart rate. In addition, NFD, HFD, and HFD-TRPV4$_{EC}^{-/-}$ mice were given a single bolus intraperitoneal injection of uric acid (200 mg/kg), FeTPPS (10 mg/kg), 1400W (10 mg/kg), or L-NNA (100 mg/kg) at noon. Sterile saline solution (0.9%) was used as a vehicle, and vehicle only injections were used as control groups for statistical comparisons. Blood pressure and heart rate were recorded for one hour, at 5-min intervals. The blood pressures, at 15-20 minutes after injection, were compared between the groups. The experiments were performed in a blinded manner.

Peroxynitrite (PN) preparation and controls. The concentration of PN in the stock solution was determined spectrophotometrically using the reported extinction coefficient for PN (1670 $mol/L^{-1}\cdot cm^{-1}$)[5]. The methods for PN preparation and use in vascular experiments were followed as published in Liu et al.[5] PN has a short half-life under physiological conditions. We, therefore, used decomposed PN as a control. Decomposed PN was obtained by leaving PN at room temperature for 2 hours[5], and the decay of PN was determined spectrophotometrically. Decomposed PN did not affect the activity of endothelial TRPV4 sparklets or vasodilation to carbachol or GSK1016790A (Supplementary Figure 25).

Ca^{2+} imaging. Ca^{2+} imaging studies were performed as described earlier[4]. Third-order MAs were surgically opened and pinned down on a SYLGARD block in *en* face preparation. MAs were incubated with fluo-4 AM (10 μM) and pluronic acid (0.04%) at 30 °C for 45 min in the dark room. Ca^{2+} images were acquired at 30 frames per second using Andor Revolution WD (with Borealis) spinning-disk confocal imaging system (Andor Technology, Belfast, UK) comprising of an upright Nikon microscope with a 60X water dipping objective (numerical aperture 1.0) and an electron multiplying charge coupled device camera. MAs were superfused with physiological salt solution (PSS; 119 mM NaCl, 4.7 mM KCl, 1.2 mM KH_2PO4, 1.2 mM $MgCl_2$ 160 hexahydrate, 2.5 mM $CaCl_2$ dihydrate, 7 mM dextrose, and 24 mM $NaHCO_3$) bubbled with 21% O_2 and 5% CO_2 to maintain the pH at 7.4. All the experiments were performed at 37°C. Fluo-4 was excited using a 488 nm solid-state laser and emitted fluorescence was captured using a 525/36 nm band-pass filter. MAs were treated with cyclopiazonic acid (CPA; 20 μM, a sarco-endoplasmic reticulum (SR/ER) Ca^{2+}-ATPase inhibitor) for 15-min at 37°C prior to imaging to eliminate intracellular Ca^{2+}release signals. CPA per se does not alter the

activity of $TRPV4_{EC}$ sparklets[4]. $TRPV4_{EC}$ sparklet activity was determined before and 5 minutes after the addition of a pharmacological agent, except in the case of GSK2193874 (GSK219, 100 nM), where the $TRPV4_{EC}$ sparklet inhibition was confirmed 10 min after incubation with GSK219.

Ca^{2+} images were analyzed using a custom-designed SparkAn software (developed by Dr. Adrian Bonev, University of Vermont). Fractional fluorescence traces (F/F_0) were obtained by placing a 1.7 μm^2 (5×5 pixels) region of interest (ROI) at the peak event amplitude. Representative F/F_0 traces were filtered using a Gaussian filter and a cutoff corner frequency of 4 Hz.

Analysis of the activity of $TRPV4_{EC}$ Ca^{2+} sparklets. Ca^{2+} signals were measured using an increase in fluorescence over the averaged image obtained from 10 images. TRPV4 Ca^{2+} sparklets were assessed based on previously established methods[6]. The average TRPV4 sparklet activity is defined as NP_O (where N is number of TRPV4 channels per site and P_O is the open state probability of the channel). NP_O was calculated using the Single Channel Search module of Clampfit, quantal amplitudes derived from all-points histograms (0.29 $\Delta F/F_0$ for fluo-4-loaded MAs), and the following equation:

$$NPo = \left[\frac{(T_{level1} + 2T_{level2} + 3T_{level3} + 4T_{level4})}{T_{total}}\right]$$

where T represents the dwell time at each quantal level and T_{total} is the total recording duration. Average NP_O per site was obtained by averaging the NP_O for all the sites in a field. Total number of sites per field indicates all the sparklet sites per field averaged over different arteries. All the sites in a field of view during the recording duration were added to obtain total number of sites per field of view.

Construction of all-points histogram. All-points histogram was constructed as described previously[7]. Briefly, images were filtered using a Kalman filter adopted from an ImageJ plug in which utilizes an acquisition noise variance estimate of 0.05 and a filter gain of 0.8 (Christopher Philip Mauer, Northwestern University, Chicago, IL). The inclusion criteria were a stable baseline containing at least five steady points and a steady peak containing at least five peak points. Sparklet traces were exported to ClampFit10.3 for constructing an all-points histogram, which was fit with the multiple Gaussian function below:

$$f(F/F_0) = \sum_{i=1}^{N} \frac{a_i}{\sqrt{2\pi\sigma_i}} \exp\left[\frac{-(\frac{F}{F_0} - \mu_i)^2}{2\sigma_i^2}\right]$$

where F/F_0 represents fractional fluorescence, a represents the area, μ represents the mean value, and $\sigma 2$ represents the variance of the Gaussian distribution. While the detected sparklets can have multiple amplitudes corresponding to quantal level 1, 2, 3, or 4, the baseline (level 0) was

the same for all the detected sparklets regardless of the amplitude of the sparklets. Therefore, the baseline corresponds to a higher count compared to all other events.

Localization analysis of TRPV4 sparklets at myoendothelial projections (MEPs). TRPV4 Ca^{2+} sparklet localization at the MEP was measured using Alexa Fluor 633 hydrazide staining of the internal elastic lamina (IEL). After performing Ca^{2+} imaging experiments, arteries were incubated with Alexa Fluor 633 hydrazide (10 μM) for 5 minutes[4]. Images were obtained from the same fields of view (matching x- and y-coordinates) that were used for recording Ca^{2+} sparklets, using an excitation wavelength of 640 nm and a band-pass emission filter (685/40 nm). Sparklet localization was assessed by overlaying the fluo-4 image with the Alexa fluor 633 IEL staining. ROIs (1.7 μm^2) corresponding to the peak sparklet fluorescence were placed on the overlaid IEL staining. Sparklet sites were considered to be localized to MEPs if the ROI was within 2 μm from the perimeter of the IEL holes[4]. The remaining sparklet sites were considered to be non-MEP sites.

Determination of coupling coefficient (κ). Coupling strength among TRPV4 channels in a cluster was determined by estimating coupling coefficients using coupled Markov chain model in Matlab, as described previously[8, 9]. Each TRPV4 sparklet event was examined separately. A single channel amplitude of 0.29 $\Delta F/F_0$ was used for fluo-4 loaded MAs based on all-points histograms and previously published data. TRPV4 channel activity was considered as a first-order, discrete Markov chain. The built-in function in Matlab for estimating Hidden Markov parameter was used to estimate a Markovian transition matrix for TRPV4 sparklets and their corresponding channel opening time course. The estimated transition matrix was modelled as a partially coupled Markov chain, revealing the coupling coefficient (κ) values that vary from 0 (no coupling or independent gating) to 1 (maximum coupling).

Immunostaining. Immunostaining was performed on *en face* MAs. Briefly, arteries were pinned down *en face* on SYLGARD blocks and fixed with 4% paraformaldehyde at room temperature for 15-min. Fixed arteries were washed 3 times with phosphate-buffered saline (PBS) solution, each wash lasting for five minutes. The arteries were then treated with 0.2% Triton-X PBS for 30-min at room temperature on a rocker. Following this step, the arteries were treated with 5% normal donkey serum or normal goat serum (Abcam plc, Cambridge, MA, USA) one hour at room temperature and subsequently incubated with antibodies against TRPV4, AKAP150, nitrotyrosine, PKC, iNOS, NOX1, NOX2, NOX4 (Table 1) overnight at 4°C. Following overnight incubation, MAs were washed three times with PBS and then incubated with secondary antibody (1:500; Alexa Fluor® 568-conjugated donkey anti-rabbit, goat anti-rabbit, or goat anti-mouse, Life Technologies, Carlsbad, CA, USA) at room temperature for one hour in the dark room. The MAs were then washed three times with PBS. For nuclear staining, MAs were incubated with 0.3 μM DAPI (Invitrogen, Carlsbad, CA, USA) for 10-min at room temperature in the dark room. Images were obtained using the Andor imaging system described previously. Consecutive images were taken along the z-axis at a slice size of 0.2-μm from the top of the ECs to the bottom of the SMCs. DAPI immunostaining was imaged by exciting at 409 nm and collecting the emitted fluorescence with a 447/60-nm band-pass filter.

The 3D rendering was accomplished using Imaris 9.3. For determining the percentage of MEPs that coincided with the immunostaining of interest (TRPV4, AKAP150, NOX, iNOS, nitrotyrosine), the total number of holes was counted for each field of view. A horizontal x-y plot profile was then obtained for each hole using 5 μm x 50 μm transects encompassing the hole. The holes that coincided with immunostaining intensity that was higher than 2 standard deviations above the baseline fluorescence intensity were counted as MEPs that expressed the protein under consideration. Other holes were grouped as MEPs that did not express the protein under consideration.

Knockout mice (TRPV4 and AKAP150), secondary antibody alone control, and blocking peptides (Novus Biologicals NBP2-54670PEP for NOX4, Proteintech Ag5536 for NOX2, custom-synthesized peptide for iNOS from GenScript) at concentration five times higher than that of the antibody were used as negative controls. Primary antibody-specific immunostaining was eliminated in secondary antibody control/blocking peptide control/knockout mice control groups.

Supplemental Table 1. A list of primary antibodies used for immunostaining.

Protein	Company	Ab ID	Clonality	Concentration
AKAP150	Santa Cruz Biotechnology, Inc.	SC 6445	Polyclonal	1:250
TRPV4	LifeSpan BioScience INC	LS_C94498	Polyclonal	1:200
iNOS	Thermofisher Scientific	PA3-030A	Polyclonal	1:1000
NOX1	Novus Biologicals, LLC	NBP1-31546	Polyclonal	1:500
NOX2	Abcam plc.	ab80508	Polyclonal	1:500
NOX4	Proteintech Group, Inc	14347-1-AP	Polyclonal	1:100
PKC	Santa Cruz Biotechnology, Inc.	SC-17769	Monoclonal	1:250
3-Nitrotyrosine	Abcam plc.	ab42789	Polyclonal	1:200
CD45	Santa Cruz Biotechnology, Inc.	sc-1178	Monoclonal	1:100
2-thiodimedone	Kerafast, Inc.	EST022	Polyclonal	1:1000

Imaging for endothelial cysteine oxidation in third-order MAs and HEK293 cells.
Reversible Cysteine sulfenic acid (CSA) intermediates of cysteine oxidation were trapped by treating the arteries with dimedone (5 mM, 60 minutes at 30°C). The arteries were then washed twice with PBS for five minutes each. Dimedone-tagged CSA containing protein were detected using anti-CSA (2-thiodimedone) antibody (Kerafast, Inc.Boston, MA, USA)[10]. The arteries

were then fixed with 4% paraformaldehyde, and the standard immunostaining, image acquisition, and analysis protocol was followed as described earlier.

For detecting PN-induced cysteine oxidation in HEK293 cells (ATCC, Manassas, VA; passages < 20), the cells were incubated with PN (10 μM) in DMEM for 5 minutes at 37°C. The cells were washed twice with PBS containing 10 mM dimedone, and then incubated with DMEM containing 10 mM dimedone for 1 hour. The cells were washed three times with PBS, and fixed with 4% paraformaldehyde. The standard immunostaining protocol was followed as explained earlier using the anti-CSA (2-thiodimedone) primary antibody. The mean fluorescence intensity for all the cells in a group was averaged per experiment. Each data point in the scatter plot indicates averaged mean fluorescence intensity per experiment. Each experiment was performed 3-5 times.

Peroxynitrite imaging. A peroxynitrite-selective fluorescent indicator coumarin boronic acid (CBA)[11] was used for peroxynitrite imaging. Peroxynitrite oxidizes CBA into the fluorescent product 7-hydroxycoumarin (COH). The arteries were incubated with CBA (20 μM) for 30 minutes at room temperature. Endothelial COH at 360 nm (CoolLED Ltd, Andover, UK); emitted fluorescence was captured at room temperature using a 447/60 nm band-pass filter, Nikon fluor 40X objective, and Andor electron multiplying charge coupled device camera. The images were analyzed using the SparkAn program. The average fluorescence intensity for the whole field was compared between the groups. Each data point indicates one field of view. At least three arteries were used for each treatment. CBA reacts with peroxynitrite at exponentially faster rates than H_2O_2 and hypochlorous acid. Moreover, the endothelial CBA fluorescence was not altered by the presence of PEG catalase (H_2O_2 decomposer) or taurine (hypochlorous acid scavenger, Supplementary Figure 11).

Cysteine sulfenic acid imaging with DCP-Rho1 in HEK293 cells. Cells were treated with PN (10 μM) in DMEM for five minutes at 37°C. The cells were then incubated with fluorescent sulfenic acid indicator DCP-Rho1 (1 μM, Kerafast, Inc.Boston, MA, USA) at 37°C for 10 minutes in DMEM containing 10 μM PN. The cells were then washed three times with PBS, and fixed with acetone:methanol (1:1) for 10 minutes at -20°C. Cells were then washed three times with PBS and incubated with DAPI (300 nM, for nuclear staining) for five minutes. DCP-Rho1 was excited at 561 nm and emitted light was captured using 607/36-nm band-pass filter. For analyzing the images, a region of interest (ROI) was drawn around each cell as seen in the brightfield images to obtain mean DCP-Rho1 fluorescence per cell. The mean fluorescence intensity for all the cells in a group was averaged per experiment. Each data point in the scatter plot indicates averaged mean fluorescence intensity per experiment. Each experiment was performed 3-5 times.

Plasmid generation and transfection of HEK293 cells. The coding sequences for murine TRPV4 and AKAP150 without the stop codons were amplified from a mouse heart cDNA and the coding sequence for EGFP from a commercially available vector. The amplified fragments were introduced into a plasmid backbone which contains a CMV promoter for expression and, in addition, is suitable for lentivirus production[12], by Gibson assembly. For TRPV4, an in-frame FLAG tag was included in the 3'-primer used for amplification. For AKAP150, the EGFP

sequence was fused to the 3' of the AKPA150 coding region. All constructs were verified by sequencing the regions, which had been inserted into the vector backbone; complete plasmid sequences are available upon request. Cells were seeded in Dulbecco's Modified Eagle Medium with 10% fetal bovine serum (Thermo Fisher Scientific Inc. Waltham, MA, USA) the day prior to transfection in a 100 mm dish (7 x 10^5 cells per dish). Cells were transfected with 15 μg plasmid using LipofectamineLTX (Thermo Fisher Scientific Inc. Waltham, MA, USA) as the transfection reagent. Patch clamp experiments were conducted 48 hours after transfection. The transfection efficiency was tested with AKAP150 or TRPV4 immunostaining. The transfection efficiency with TRPV4 plasmid was ~ 96%, and that with AKAP150 plasmid was ~ 50%. For patch clamp experiments, the cells carrying AKAP150 were identified by EGFP fluorescence.

Site-directed mutagenesis: The mouse AKAP150 sequence inserted into a pLenti CMV GFP plasmid was synthesized as described above. For mutagenesis, cysteine to alanine primers were designed against residue 36 (C36A) using the QuikChange primer design program, and mutagenesis performed using the QuikChange II site-directed mutagenesis kit as per manufacturer instructions (Agilent, Stratagene, Santa Clara, CA). Primers for mutations are as follows: forward 5' ctttcttccttctcttgaaggcgagtgtggctgtttttctct 3' and reverse: 5' agagaaaaacagccacactcgccttcaagagaaggaagaaag 3' (IDT, Coralville, IA). Mutants were sequenced (GeneWiz, South Plainfield, NJ), confirmed and maxi prepped for transfection studies. Sequencing confirmed the $AKAP150^{C36A}$ mutation.

Patch Clamp in freshly isolated ECs and HEK293 cells. ECs were freshly isolated from third-order MAs. Briefly, MAs were digested in dissociation solution (55 mM NaCl, 80 mM Na-glutamate, 6 mM KCl, 2 mM $MgCl_2$, 0.1 mM $CaCl_2$, 10 mM glucose, 10 mM Hepes, pH 7.3) containing Worthington neutral protease (0.5 mg/mL) 60 minutes at 37°C. Collagenase (Worthington type 1, 0.5 mg/mL) was added to the enzyme solution after 60 minutes and digestion was continued for 2 more minutes. Whole-cell currents were measured at room temperature using perforated-patch configuration of whole-cell patch clamp. The bathing solution consisted of 10 mM Hepes, 134 mM NaCl, 6 mM KCl, 2 mM $CaCl_2$, 10 mM glucose, and 1 mM $MgCl_2$ (adjusted to pH 7.4 with NaOH). Patch electrodes were pulled from borosilicate glass (O.D.: 1.5 mm; I.D.: 1.17 mm; Sutter Instruments, Novato, CA, USA) using Narishige PC-100 puller (Narishige International USA, INC., Amityville, NY, USA) and polished using MicroForge MF-830 polisher (Narishige International USA, INC., Amityville, NY, USA). The composition of the pipette solution for perforated-patch experiments was 10 mM Hepes, 30 mM KCl, 10 mM NaCl, 110 mM K-aspartate, and 1 mM $MgCl_2$ (adjusted to pH 7.2 with NaOH). IK and SK channels currents were obtained by adding 1 μM NS309 (IK/SK channel activator) to the superfusate. The pipette resistance was (3–5 ΩM). Currents were recorded by applying 200 ms voltage-ramps from −140 mV to +50 mV. The data were acquired using HEKA EPC 10 amplifier and PatchMaster v2X90 program (Harvard Bioscience, Holliston, MA, USA). The patch clamp data were analyzed using FitMaster v2X73.2 (Harvard Bioscience, Holliston, MA, USA) and MATLAB R2018a (MathWorks, Natick, MA, USA). IK/SK channel currents were inhibited by adding Tram-34 (IK channel inhibitor, 1 μM) and apamin (SK channel inhibitor, 300 nM) to the bath. Current traces in the presence of Tram-34 and apamin

were subtracted from the traces in the presence of NS309 alone to obtain IK/SK channel currents. The effect of each drug was studied 5 minutes after the addition of the drug.

Currents through TRPV4 channels in freshly isolated ECs were recorded using perforated patch configuration as described earlier[7]. Ruthenium red (RuR, 1 μM) was applied to block Ca^{2+} entry through TRPV4 channels, and thereby prevent IK and SK channel activation and Ca^{2+} overload. GSK101-induced outward currents through TRPV4 channels were assessed in response to a 200-ms voltage step from -45 mV to +100 mV. The cells were exposed to GSK101, PN, or GSK219 for 5 minutes before recording the currents.

For HEK293 cells patch clamp, whole-cell currents were measured at room temperature using a conventional whole-cell patch configuration. The bathing solution consisted of 10 mM Hepes, 134 mM NaCl, 6 mM KCl, 2 mM $CaCl_2$, 10 mM glucose, and 1 mM $MgCl_2$ (adjusted to pH 7.4 with NaOH). The intracellular solution consisted (in mM) 20 CsCl, 100 Cs-aspartate, 1 $MgCl_2$, 4 ATP, 0.08 $CaCl_2$, 10 BAPTA, 10 Hepes, pH 7.2 (adjusted with CsOH). Voltage clamped protocol used was voltage-ramp pulses (-100 mV to +100 mV) applied over 200 ms with a holding potential of -50 mV. TRPV4 currents were measured before or five minutes after the addition of 5 μM peroxynitrite. The effect of TRPV4 inhibitor GSK2193874 (GSK219, 100 nM) was studied by recording currents before and 5 minutes after addition of GSK219.

Quantitative polymerase chain reaction (qPCR). Third-order MAs were removed, placed in 500 μL RLT buffer (Qiagen RNeasy Mini Kit, Hilden, Germany) with 5 μL β-mercapto ethanol, and homogenized using a Standard Microhomogenizer (PRO Scientific Inc., Oxford, CT, USA). For isolation of RNA from endothelial cells, approximately 20 mesenteric arteries from each mouse were used. Arteries were digested in a dissociation solution containing (0.5 mg/mL) 60 minutes at 37°C. Collagenase (Worthington type 1, 0.5 mg/mL) was added to the enzyme solution after 60 minutes and digestion was continued for 2 more minutes. Following the digestion, endothelial cell sheets were gently pushed out of the arterial wall using fine tips of 1 mL syringe needles. Isolated endothelial cell sheets were then placed in a patch clamp chamber, allowed to settle down for 15 minutes at room temperature, and washed three times with enzyme-free dissociation buffer. Endothelial cell sheets were then picked up using a micropipette (~ 100 μm tip) under gentle suction, and transferred to a tube with RLT buffer with β-mercapto ethanol for RNA isolation. The steps were repeated in order to pick several endothelial cell sheets. Approximately 20 sheets were used for each sample. Each sheet has approximately 100 cells. The purity of endothelial cells was confirmed with FITC-labelled anti-CD31 antibody. The RLT buffer (with β-mercapto ethanol and endothelial cell sheets) was snap frozen in liquid nitrogen. The samples were thawed, RNA was isolated using a Qiagen RNeasy Mini Kit (Hilden, Germany), treated with Invitrogen DNA-free DNA Removal Kit (Waltham, MA), and converted to cDNA with Bio-Rad iScript cDNA Synthesis Kit. The qPCR reaction mixes were prepared using Bio-Rad 2x SYBR Green Master Mix, 200nM 5' and 3' primers, and 20 nM cDNA, then run in a Bio-Rad CFX96 qPCR Detection System. Results were analyzed using the $\Delta\Delta C_t$ Method[13]. qPCR primers for TRPV4 and GAPDH (internal control) were ordered from GeneCoepia Inc. (Rockville, MD, USA). The remaining qPCR primers included: AKAP150, 5' GACCTCGGGAGCAGAGC, 3' CTTGAAGCAGAGTGTGGCT; iNOS, TTCACCCAGTTGTGCATCGACCTA, 3' TGGGCTGGGTGTTAGTCTTA; NOX1, 5'

ACCTGCTCATTTTGCAACCGTA, 3' AGAGATCCATCCATGGCCTGTT, and were ordered from Eurofins Genomics (Louisville, KY).

Proximity Ligation Assay (PLA). Third-order MAs were isolated and pinned down *en face* on SYLGARD block. Arteries were fixed in paraformaldehyde (4%) for 15 minutes and then washed three times with PBS. Arteries were then incubated in a solution of 0.2% Triton X for 30 minutes at room temperature. After that arteries were blocked either with 5% normal donkey serum (Abcam plc, Cambridge, MA, USA) and 300 mM glycine at room temperature for one hour. Lastly, arteries were washed three time with PBS and incubated overnight at 4°C with primary antibodies. The following day, PLA protocol from Duolink PLA Technology kit (Sigma-Aldrich, St. Louis, MO, USA) was followed and finally arteries were treated with 0.3 μM DAPI nuclear staining (Invitrogen, Carlsbad, CA, USA) for 10-min at room temperature in the dark room. PLA imaging was conducted using Andor Revolution spinning-disk confocal imaging system and analyzed with a Duolink Image Tool (Sigma-Aldrich, St. Louis, MO, USA). Images were obtained along the z-axis at a slice size of 0.02 μm from the top of the endothelial cells to the bottom of the smooth muscle cells. Knockout mice and secondary antibody alone was used as negative controls for the PLA experiments.

Nitric oxide (NO) measurements. *En face* MAs on a Sylgard block were incubated with 5 μM DAF-FM (4-amino-5 methylamino-2',7'-difluorofluorescenin diacetate) prepared in Hepes PSS with 0.02% pluronic acid[14] for 20 minutes at 30˚C in the dark. DAF-FM forms a fluorescent triazole compound after binding to NO. DAF-FM fluorescence was imaged using Andor Revolution WD (with Borealis) spinning-disk confocal imaging system. DAF-FM fluorescence was recorded using an excitation wavelength of 488 nm and emitted fluorescence was captured with a 525/36-nm band-pass filter. Images were obtained along the z-axis at a slice size of 0.05 μm from the top of the endothelial cells to the bottom of the smooth muscle cells. DAF-FM fluorescence was analyzed using custom-designed SparkAn software by. An outline was drawn around each endothelial cell to obtain the arbitrary fluorescence intensity of that cell. The background fluorescence was then subtracted from the recorded fluorescence. The fluorescence numbers from all the cells in a field of view were averaged to obtain single fluorescence number for that field.

Measurement of $O_2^{\cdot-}$ production in MAs. Dihydroethidium (DHE, Thermo Fisher Scientific Inc. Waltham, MA, USA) was used for detecting $O_2^{\cdot-}$ generation in *en face* MAs on a SYLGARD block. The MAs were incubated with DHE (2 μM) in the dark at 30°C for 30 min. Following the incubation, the arteries were washed three times with Hepes PSS, and then fixed in 4% paraformaldehyde for 20 minutes at room temperature. Images were acquired using the Andor Imaging system described above. Images were obtained along the z-axis at a slice size of 0.05 μm from the top of the endothelial cells to the bottom of the smooth muscle cells. Endothelial cell fluorescence intensity was quantified using custom-made SparkAn software.

Hypochlorous acid imaging. A selective fluorescent probe (PIS, Millipore Sigma, Burlington, MA, USA)[15] was used for imaging endothelial hypochlorous acid in non-obese and obese mice. The arteries were incubated with PIS for 60 minutes at 30°C. The images were acquired at room

temperature by exciting PIS at 385 nm and capturing the emitted fluorescence using 525/36 nm band-pass filter and Andor EMCCD camera.

Drugs and chemical compounds. Cyclopiazonic acid, GSK1016790A, GSK2193874, NS309, apamin, charybdotoxin, tempol, Phorbol 12-myristate 13-acetate, and ML-171 were purchased from Tocris Bioscience (Minneapolis, MN, USA). PEG-catalase, L-NNA, CCh, Alexa fluor 633 hydrazide, and DAF-FM were procured from Thermo Fisher Scientific Inc. (Waltham, MA, USA). gp91 ds – tat was obtained from AnaSpec (Fremont, CA, USA). PN, UA, FeTPPS, ML-171, and 1400w were purchased from Cayman Chemical (Ann Arbor, MI, USA). All other chemicals were purchased from Sigma-Aldrich (St. Louis, MO, USA).

Statistical Analysis. Results are presented as mean ± SEM. N=1 was defined as one artery in the imaging experiments (Ca^{2+} imaging, immunofluorescence, PN/NO/superoxide/hypochlorous acid measurements, PLA, DCP-Rho1), one cell for patch clamp experiments, one mouse for blood pressure measurements, one artery for pressure myography experiments, one sparklet site for coupling coefficient analysis, and one mouse for qPCR experiments. The data were obtained from at least three mice in experiments performed in at least two independent batches. All data are shown in graphical form using CorelDraw Graphics Suite X7 (Ottawa, ON, Canada) and statistically analysed using GraphPad Prism 8.3.0 (Sand Diego, CA). A power analysis to determine group sizes and study power (>0.8) was calculated using GLIMMPSE software (α = 0.05; >20% change). Using this method, some experiments required n=3, while others required n≥4. A Shapiro-Wilk test was performed to determine normality. The data in this article were normally distributed; therefore, parametric statistics were performed. Data were analyzed using two-tailed, paired or independent t-test (for comparison of data collected from two different treatments), one-way ANOVA or two-way ANOVA (to investigate statistical differences among more than two different treatments). Tukey correction was performed for multiple comparisons with one-way ANOVA, and Bonferroni correction was performed for multiple comparisons with two-way ANOVA. Statistical significance was determined as a *P* value less than 0.05; $*P < 0.05$, $** P < 0.01$, $*** P < 0.001$. Similarly, $^{\#} P < 0.05$, $^{\#\#} P < 0.01$, $^{\#\#\#} P < 0.001$.

SUPPLEMENTAL DATA

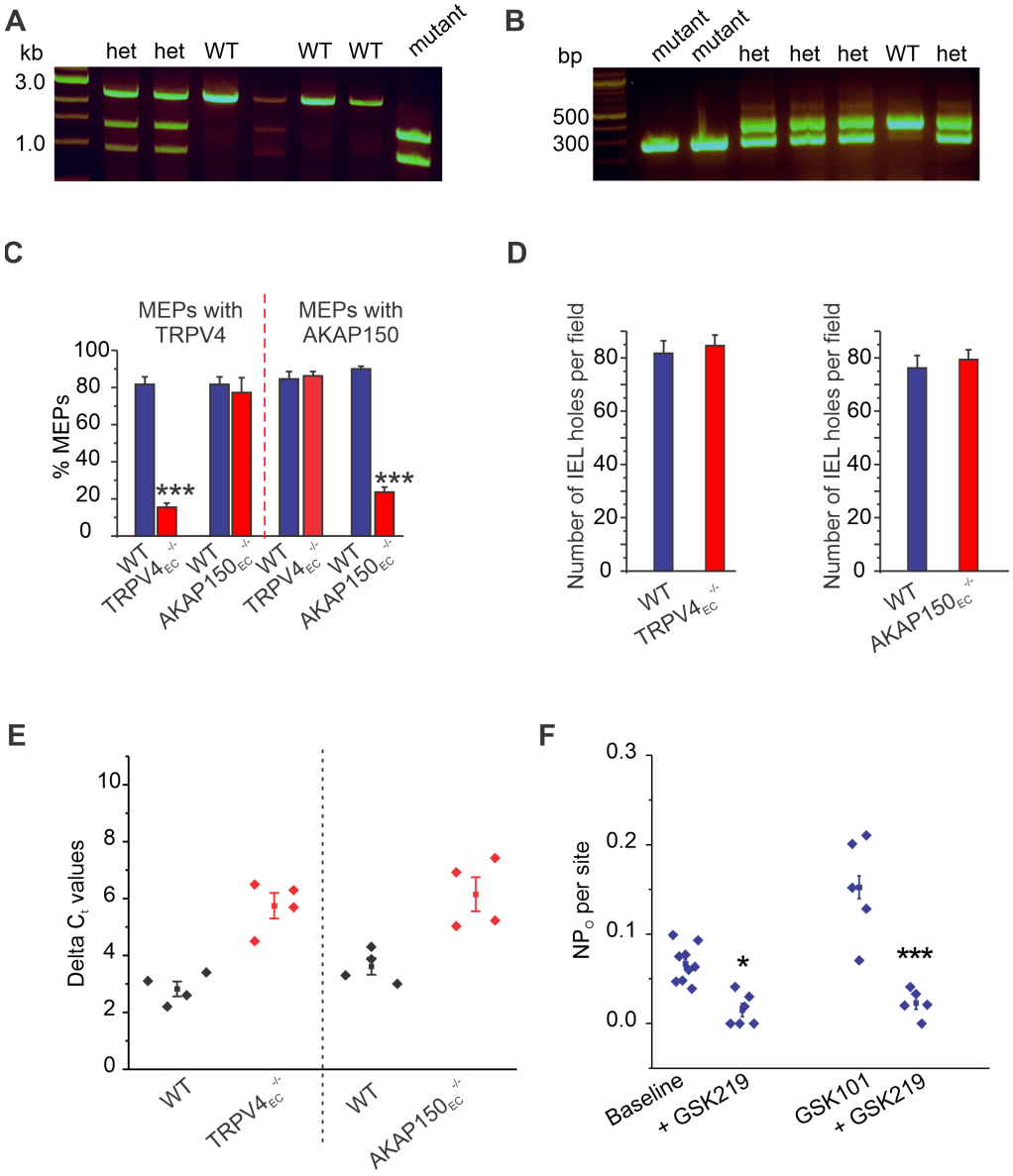

Supplemental Figure 1. TRPV4$_{EC}$ and AKAP150$_{EC}$ levels are reduced in TRPV4$_{EC}^{-/-}$ and AKAP150$_{EC}^{-/-}$ mice, respectively, but not the MEPs. Representative gel images showing genotyping data for TRPV4^{lox} (A) and AKAP150^{lox} (B), WT, wild-type; mutant, TRPV4$^{lox/lox}$ or AKAP150$^{lox/lox}$; het or heterozygous, TRPV4$^{lox/WT}$ or AKAP150$^{lox/WT}$. (C) Quantification of TRPV4$_{EC}$ (*left*) or AKAP150$_{EC}$ (*right*) immunostaining at the myoendothelial projections (MEPs) in TRPV4$_{EC}^{-/-}$ or AKAP150$_{EC}^{-/-}$ mice and respective WT mice (mean±SEM, n=5; $P <$ 0.001 versus WT, one-way ANOVA). (D) Quantification of number of holes in the internal elastic lamina (IEL) in MAs of WT mice compared with TRPV4$_{EC}^{-/-}$ mice (*left*) and AKAP150$_{EC}^{-/-}$ mice (*right*) (n=5). (E) Delta C_t values from qPCR experiments for endothelial mRNA for

TRPV4 channel (left) and AKAP150 (right) from WT and $TRPV4_{EC}^{-/-}$ or $AKAP150_{EC}^{-/-}$ mice (n=4). (F) Averaged $TRPV4_{EC}$ sparklet activity (NP_O) at MEP locations in MAs from WT mice in the absence or presence of TRPV4 channel inhibitor GSK2193874 (GSK219, 100 nM) and activator GSK1016790A (GSK101, 10 nM), $*P < 0.05$ for baseline versus GSK219, ***< 0.001 for GSK101 versus GSK219, one-way ANOVA (n=5-9).

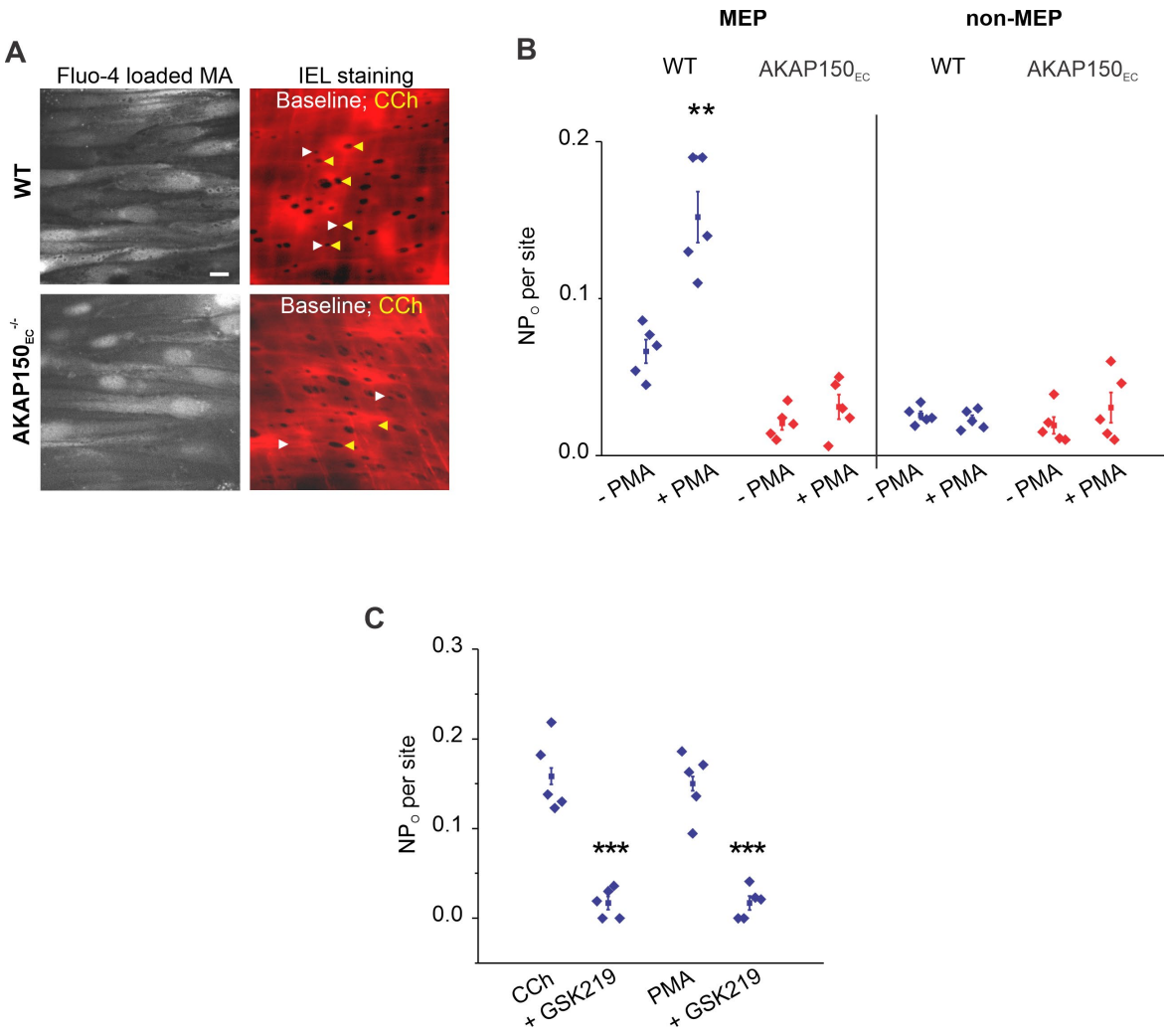

Supplemental Figure 2. TRPV4$_{EC}$ sparklet activation at MEPs is impaired in AKAP150$_{EC}^{-/-}$ mice. (A) Representative fields of view showing ECs from *en face* MAs loaded with fluo-4 (*left*) and the same fields counterstained with Alexa Fluor 633 hydrazide (*right*) for visualizing the IEL. White arrows indicate TRPV4$_{EC}$ sparklet sites under baseline conditions (cyclopiazonic acid or CPA, 20 μM) and yellow arrows indicate TRPV4$_{EC}$ sparklet sites in the presence of carbachol (CCh; 10 μM). Scale: 10 μm. (B) Averaged TRPV4$_{EC}$ sparklet activity (NP_O) at MEP and non-MEP locations in MAs from WT and AKAP150$_{EC}^{-/-}$ mice under baseline conditions, or in response to phorbol-12-myristate-13-acetate (PMA, 10 nM); $^{**}P < 0.01$ versus –PMA WT, one-way ANOVA, n=5. (C) Averaged TRPV4$_{EC}$ sparklet activity (NP_O) at MEP locations in MAs from WT mice in the absence or presence of TRPV4 channel inhibitor GSK2193874 (GSK219, 100 nM), ***< 0.001 for CCh/PMA versus GSK219, one-way ANOVA (n=5).

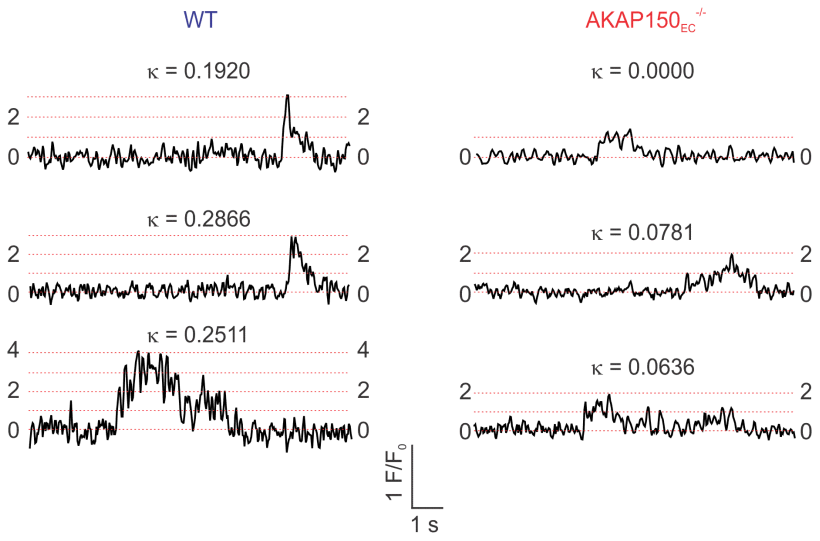

Supplemental Figure 3. Coupling strength among TRPV4 channels at a site is reduced in AKAP150$_{EC}^{-/-}$ mice. Representative baseline F/F_0 traces from TRPV4$_{EC}$ sparklet sites localized at the MEPs in fluo4-loaded MAs from WT (*left*) and AKAP150$_{EC}^{-/-}$ (*right*) in the presence of cyclopiazonic acid (CPA, 20 μM). Dotted red lines indicate the quantal levels (i.e. stepwise openings of 1–4 TRPV4$_{EC}$ channels at a site[7]) derived from all-points histogram (Extended data Fig. 8). The corresponding coupling coefficients (κ) are shown at the top of each trace.

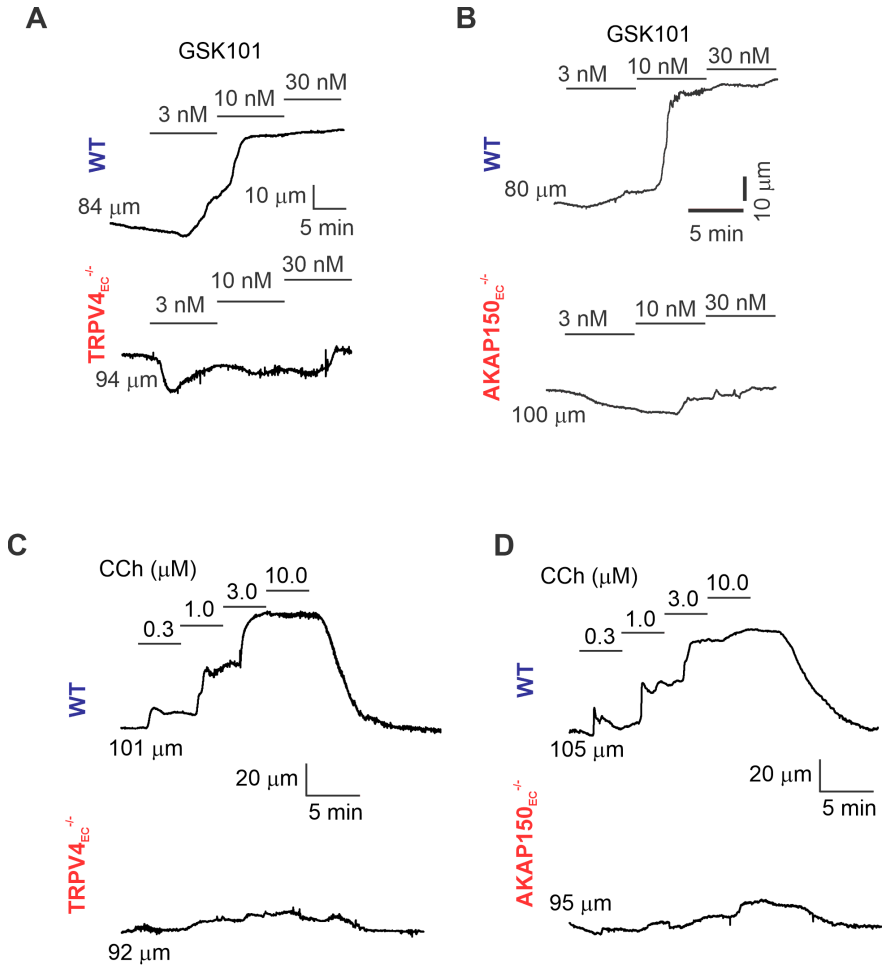

Supplemental Figure 4. CCh- and GSK101-induced vasodilation is markedly reduced in mesenteric arteries (MAs) from TRPV4$_{EC}^{-/-}$ and AKAP150$_{EC}^{-/-}$ mice. (A) Representative diameter traces for GSK101-induced vasodilation in MAs from WT (*top*) and TRPV4$_{EC}^{-/-}$ (*bottom*) mice. (B) Representative diameter traces for GSK101-induced vasodilation in MAs from WT (*top*) and AKAP150$_{EC}^{-/-}$ (*bottom*) mice. (C) Representative diameter traces for carbachol (CCh) -induced vasodilation in MAs from WT (*top*) and TRPV4$_{EC}^{-/-}$ (*bottom*) mice. (D) Representative diameter traces for carbachol (CCh) -induced vasodilation in MAs from WT (*top*) and AKAP150$_{EC}^{-/-}$ (*bottom*) mice.

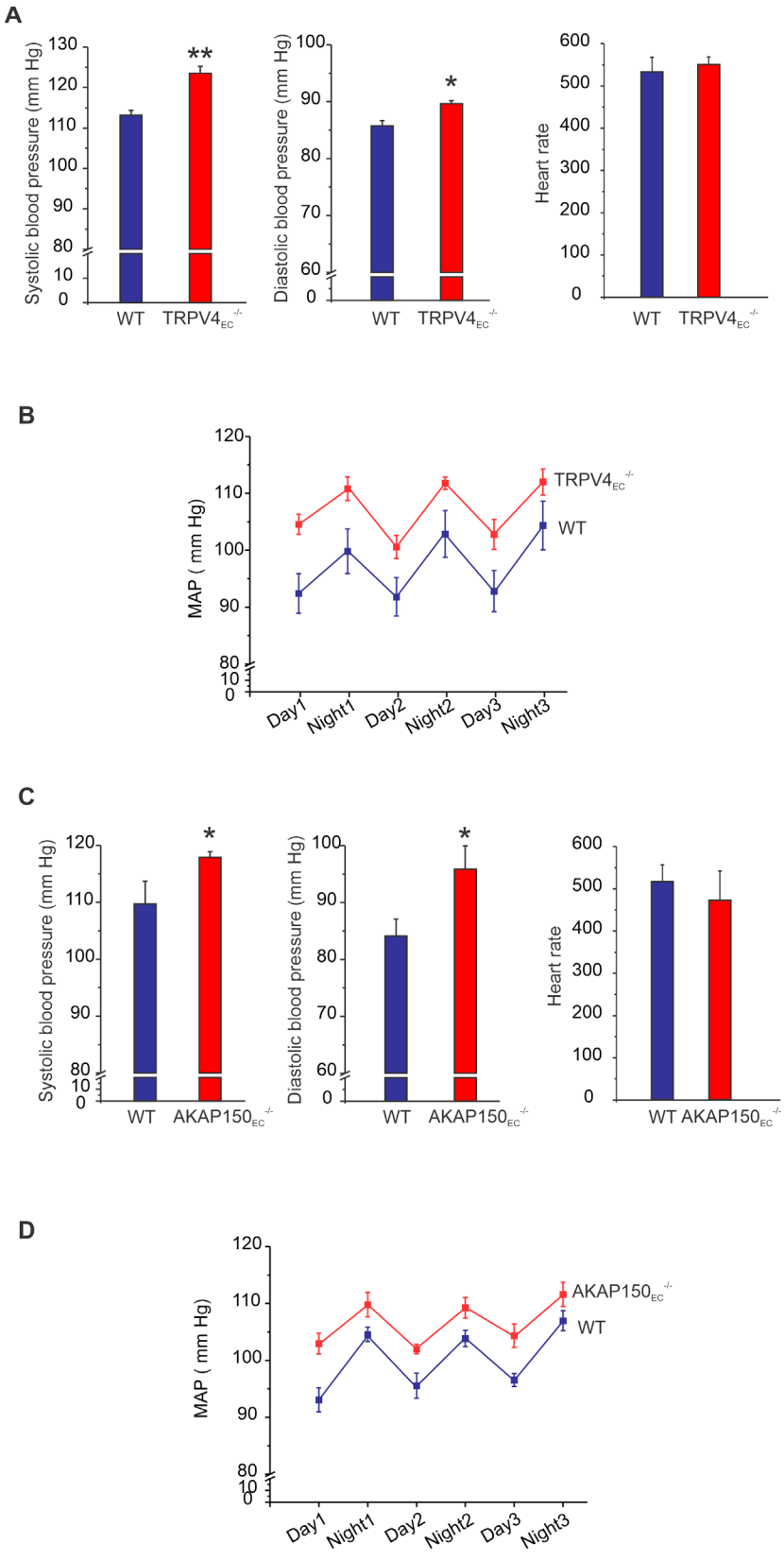
A
Systolic blood pressure (mm Hg)
130
120
110
100
90
80
10
0
**
WT
TRPV4EC-/-
Diastolic blood pressure (mm Hg)
100
90
80
70
60
0
*
WT
TRPV4EC-/-
Heart rate
600
500
400
300
200
100
0
WT
TRPV4EC-/-
B
MAP (mm Hg)
120
110
100
90
80
10
0
TRPV4EC-/-
WT
Day1
Night1
Day2
Night2
Day3
Night3
C
Systolic blood pressure (mm Hg)
120
110
100
90
80
10
0
*
WT
AKAP150EC-/-
Diastolic blood pressure (mm Hg)
100
90
80
70
60
0
*
WT
AKAP150EC-/-
Heart rate
600
500
400
300
200
100
0
WT
AKAP150EC-/-
D
MAP (mm Hg)
120
110
100
90
80
10
0
AKAP150EC-/-
WT
Day1
Night1
Day2
Night2
Day3
Night3

Supplemental Figure 5. Endothelium-specific knockout of TRPV4 or AKAP150 alters hemodynamic responses. (A) Quantification of systolic blood pressure (mm Hg, data are mean±SEM, n=5, $^{**}P < 0.01$, t-test, *left*), diastolic blood pressure (n=5, $^{*}P < 0.05$, t-test, *middle*) and heart rate (*right*, n=5) in $TRPV4_{EC}^{-/-}$ mice compared to WT. (B) Resting mean arterial pressure (MAP, mmHg) recorded over three days and three nights in WT and $TRPV4_{EC}^{-/-}$ mice (n=5). (C) Quantification of systolic blood pressure (n=5, $^{*}P < 0.05$, t-test, *left*), diastolic blood pressure (*middle*, n=5, $^{*}P < 0.05$, t-test) and heart rate (right, n=5) in $AKAP150_{EC}^{-/-}$ mice compared to WT. (D) Resting mean arterial pressure (MAP, mmHg) recorded over three days and three nights in WT and $AKAP150_{EC}^{-/-}$ mice.

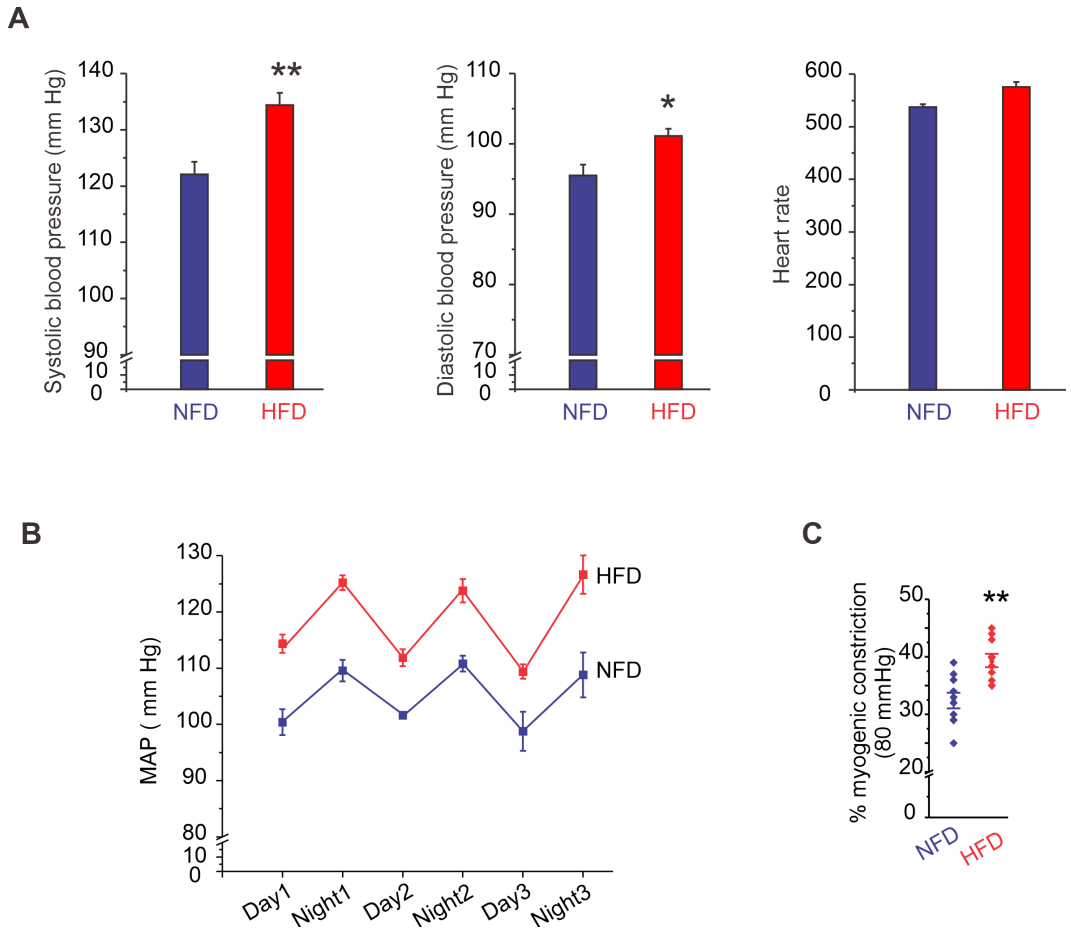

Supplemental Figure 6. Diet-induced obesity elevates blood pressure. (A) Quantification of systolic blood pressure (n=5, $^{**}P < 0.01$, t-test, *left*), diastolic blood pressure (n=5, $^{*}P < 0.05$, t-test, *middle*) and heart rate (*right*) in high fat diet (HFD)-fed mice compared to normal fat diet-fed (NFD) mice. (B) Mean arterial pressure (MAP, mmHg) recorded over three days and three nights in NFD and HFD mice (n=5). (C) Percent myogenic constriction at 80 mm Hg in MAs from NFD and HFD mice ($^{**}P < 0.01$, t-test, n=10).

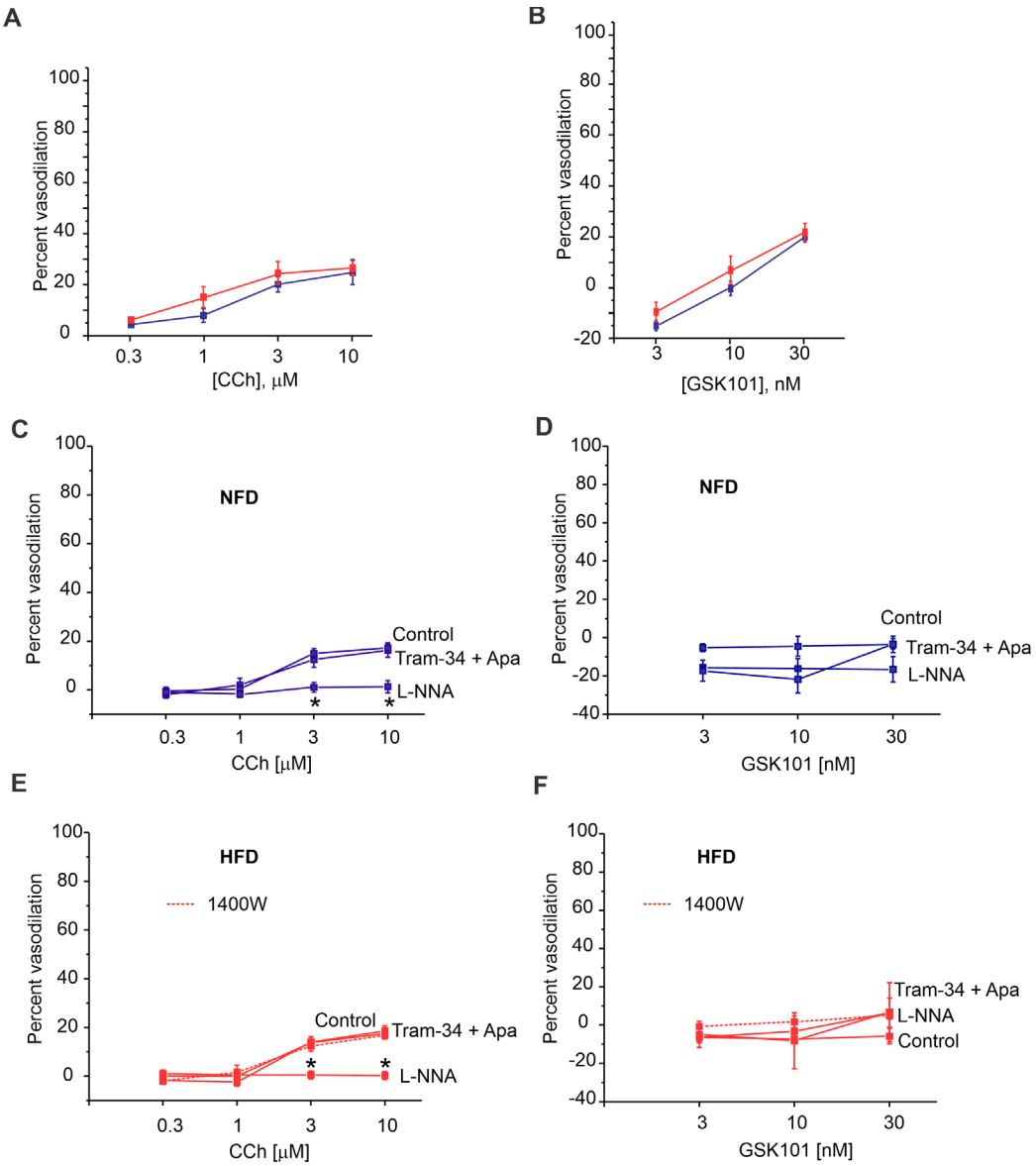

Supplemental Figure 7. IK/SK channel-independent vasodilation is unaltered in obesity. Percent dilation of MAs from NFD (blue) and HFD (red) mice in response to CCh (0.3–10 μM) (*A*) and GSK101 (3-30 nM) (*B*) (n = 5) in the presence of Tram-34 (IK channel inhibitor, 1 μM) and Apamin (SK channel inhibitor, 300 nM). (C) Percent dilation of MAs from NFD mice superfused with 60 mM K^+ physiological salts solution (PSS) in response to CCh (0.3–10 μM) in the absence or presence of Tram-34 and Apamin, or L-NNA (100 μM) (n=5, **P*< 0.05 vs. Control at 3 and 10 μM CCh; two-way ANOVA). (D) Percent dilation of MAs from NFD mice superfused with 60 mM K^+ physiological salts solution (PSS) in response to GSK101 (3–30 nM) in the absence or presence of Tram-34 and Apamin, or L-NNA (100 μM). (E) Percent dilation of MAs from HFD mice superfused with 60 mM K^+ physiological salts solution (PSS) in response to CCh (0.3–10 μM) in the absence or presence of Tram-34 and Apamin, L-NNA (100 μM), or 1400W (1 μM, dotted line) (n=5, **P*< 0.05, at 3 and 10 μM CCh; two-way ANOVA). (F) Percent dilation of MAs from HFD mice superfused with 60 mM K^+ PSS in response to GSK101 (3–

30 nM), in the absence or presence of Tram-34 and Apamin, L-NNA (100 μM), or 1400W (1 μM, dotted line), n=5.

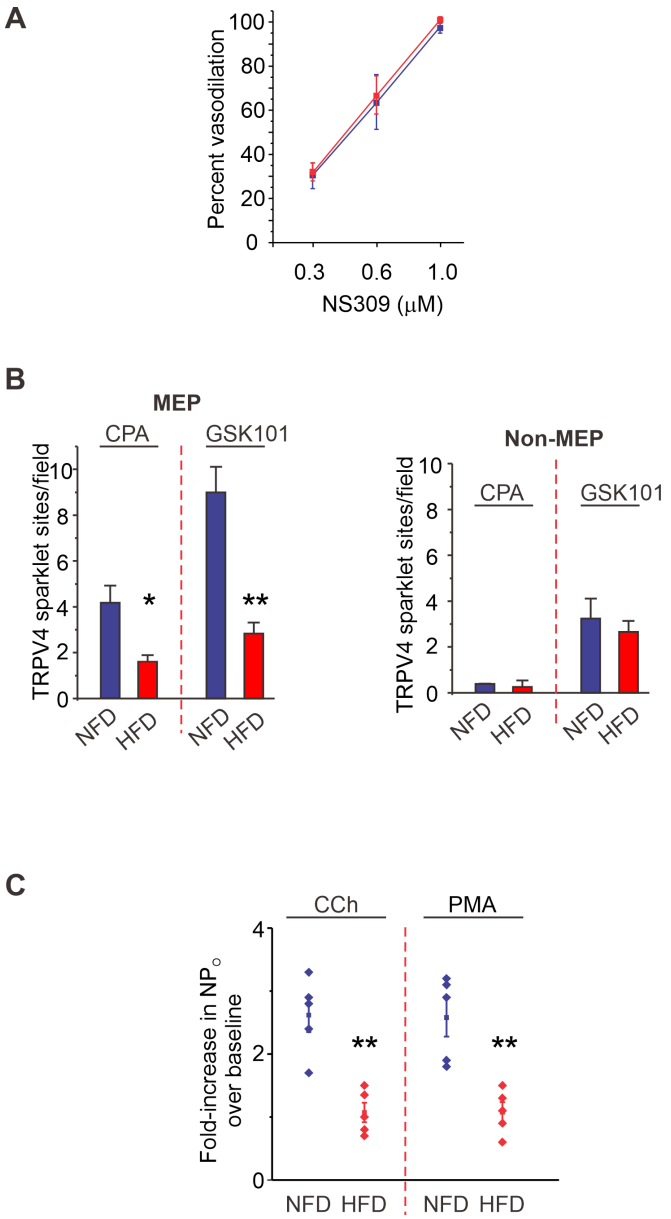

Supplemental Figure 8. Diet-induced obesity lowers TRPV4$_{EC}$ channel activity, but does not affect IK/SK channel-induced vasodilation. (A) Averaged diameter data for NS309 (0.3–1.0 μM)-induced dilation of MAs from NFD and HFD mice (n = 5). (B) TRPV4$_{EC}$ sparklet sites per field of view at the MEP (*right*) and non-MEP (*left*) sites (sparklet sites/field: ***$P < 0.001$ for NFD vs. HFD; t-test). (C) Scatter plot showing fold increases in TRPV4$_{EC}$ sparklet activity (NP_O) at MEP sites relative to baseline in the presence of CCh (10 μM) or PMA (10 nM) in MAs from NFD and HFD mice (n = 5; **$P < 0.01$ for NFD vs. HFD; one-way ANOVA).

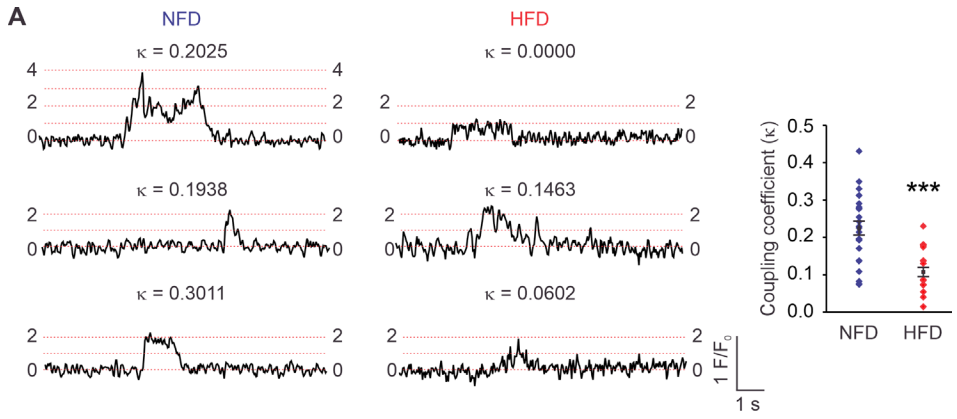
A
NFD
HFD
κ = 0.2025
κ = 0.0000
κ = 0.1938
κ = 0.1463
κ = 0.3011
κ = 0.0602
Coupling coefficient (κ)
***
NFD
HFD
1 F/F0
1 s

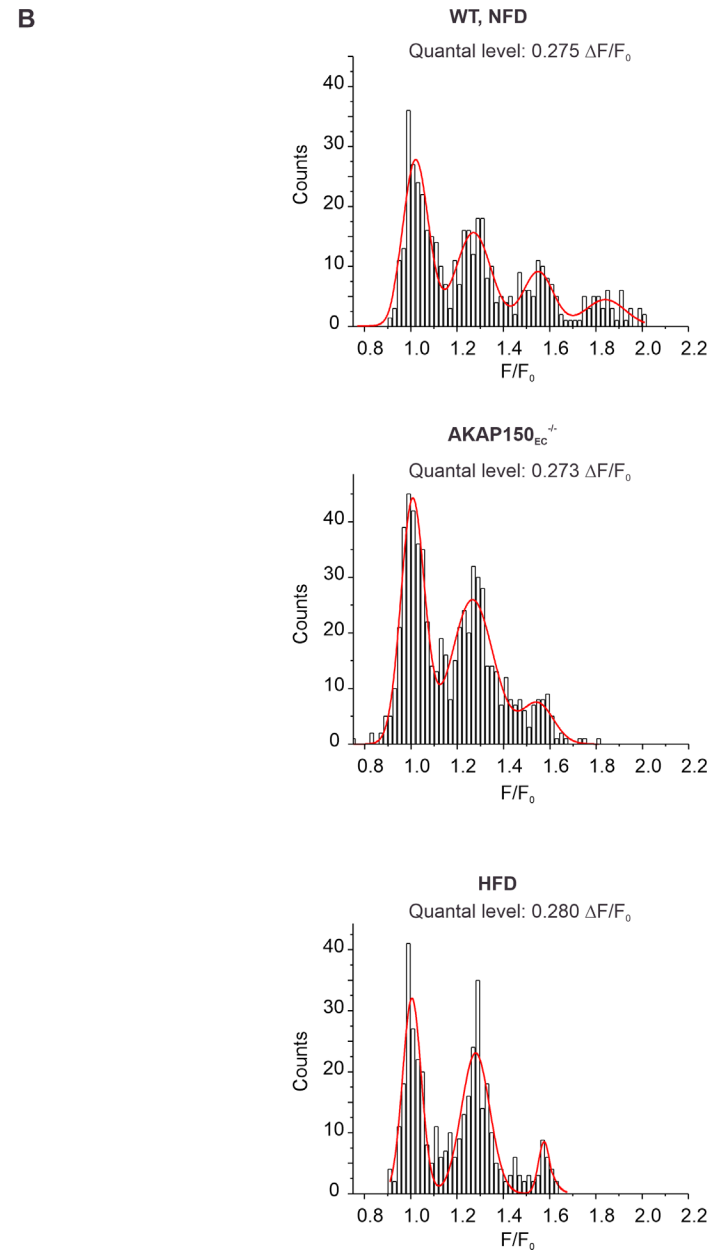
B
WT, NFD
Quantal level: 0.275 ΔF/F0
AKAP150ec-/-
Quantal level: 0.273 ΔF/F0
HFD
Quantal level: 0.280 ΔF/F0
Counts
F/F0

Supplemental Figure 9. AKAP150$_{EC}$ knockout or high fat diet feeding does not alter the quantal level of TRPV4$_{EC}$ sparklets in mesenteric arteries (MAs). (A) Representative F/F_0 traces (*left*) with corresponding κ (coupling coefficient) values for three distinct TRPV4$_{EC}$ sparklet sites in fluo4-loaded MAs from NFD and HFD mice. Dotted red lines indicate the quantal levels (i.e. stepwise openings of 1–4 TRPV4$_{EC}$ channels at a site). The κ values vary from 0 (no coupling or independent gating) to 1 (maximum coupling). Averaged coupling coefficient (κ) values (*right*) for TRPV4$_{EC}$ sparklet sites at MEP locations indicating the coupling strength among TRPV4$_{EC}$ channels at given sites in MAs from NFD and HFD mice (n = 25–29 sites; ***$P < 0.001$; t-test). (B) All-points histograms were made from F/F_0 traces obtained from MAs of WT (*top*), AKAP150$_{EC}^{-/-}$ (*middle*) and HFD (*bottom*) mice. They were fit with a multi-Gaussian curve. The quantal levels (i.e. step-wise increases in amplitudes) were obtained from the peaks of the multi-Gaussian curve.

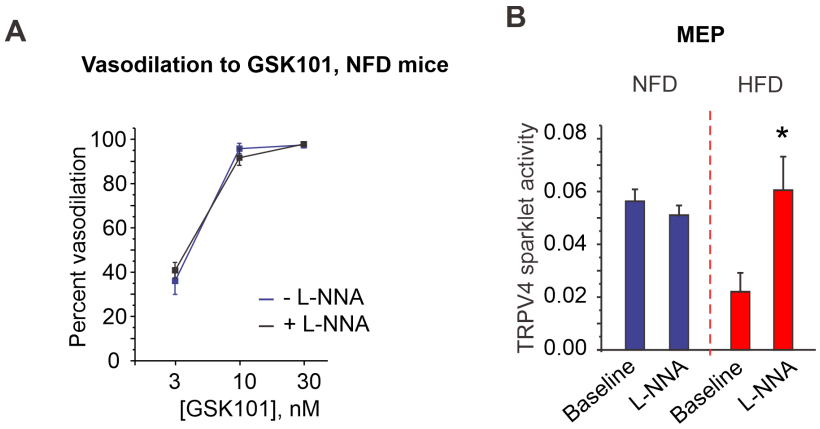

Supplemental Figure 10. Pharmacological inhibition of nitric oxide synthase does not alter TRPV4$_{EC}$ sparklet activity or TRPV4$_{EC}$-mediated vasodilation in normal (NFD) mice. (A) Averaged diameter data for GSK101-dose response curve in MAs from NFD mice in presence or absence of L-NNA (100 μM, n=5). (B) Averaged basal TRPV4$_{EC}$ sparklet activity (NP_O) at the MEPs in MAs from NFD and HFD mice in the presence or absence of L-NNA (100 μM, n=5, *$P < 0.05$ for L-NNA vs. baseline in HFD mice; one-way ANOVA).

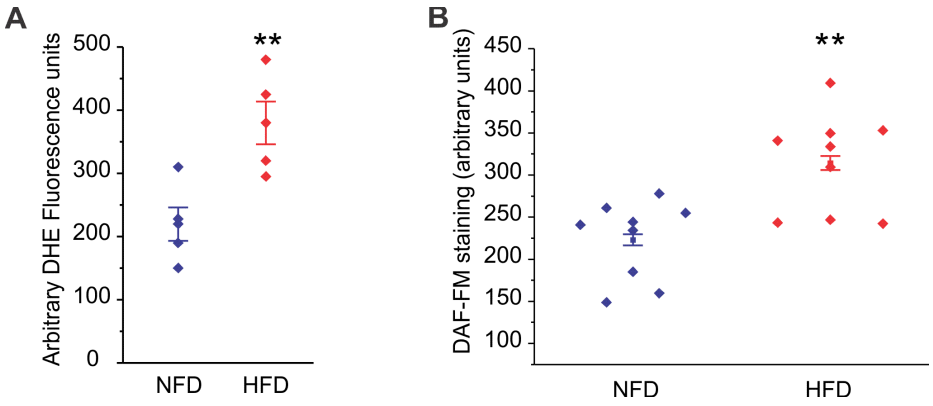

Supplemental Figure 11. Endothelial reactive oxygen species and nitric oxide (NO) levels are elevated in mesenteric arteries (MAs) from obese (HFD) mice. (A) Averaged arbitrary fluorescence of dihydroethidium (DHE) in MAs from NFD and HFD mice (n=5, **P < 0.01, t-test). (B) Averaged DAF-FM (4-amino- 5 methylamino- 2′,7′- difluorofluorescenin diacetate) fluorescence in ECs from normal (NFD) and HFD mice (n=9, **P < 0.01, t-test).

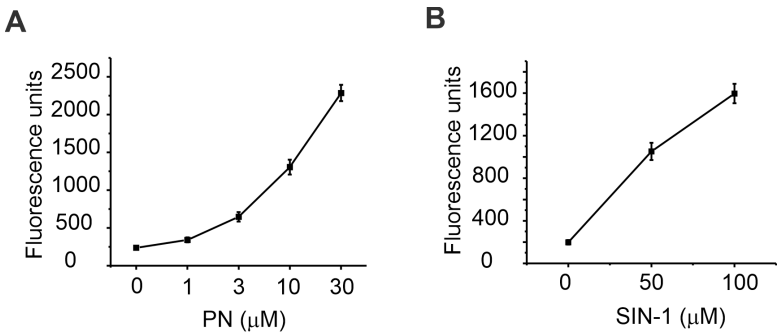

Supplemental Figure 12. Peroxynitrite (PN) and PN generator SIN-1 increase coumarin boronic acid (CBA) fluorescence in a concentration-dependent manner. (A) Averaged CBA fluorescent intensity in ECs from mouse mesenteric arteries (MAs) in the absence or presence of PN (0-30 μM; n=3). (B) Averaged CBA fluorescence intensity in ECs from mouse MAs in the absence or presence of SIN-1 (50 μM and 100 μM; n=3).

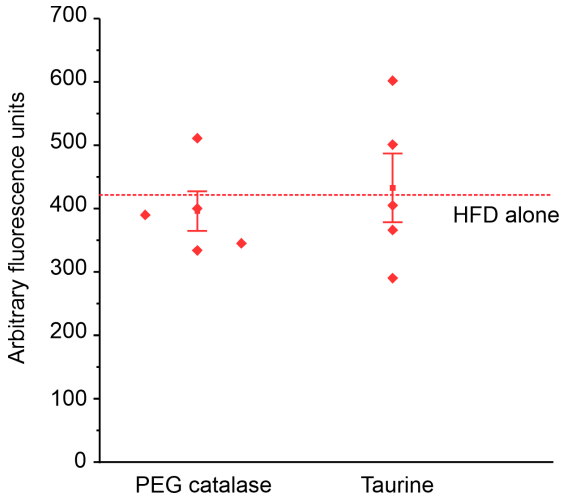

Supplemental Figure 13. Hydrogen peroxide and hypochlorous acid do not increase peroxynitrite levels in HFD mice. Endothelial arbitrary fluorescence of coumarin boronic acid (CBA) in MAs from HFD mice (dotted line) and in MAs from HFD mice in the presence of hydrogen peroxide decomposer PEG catalase and hypochlorous acid scavenger taurine, n=5.

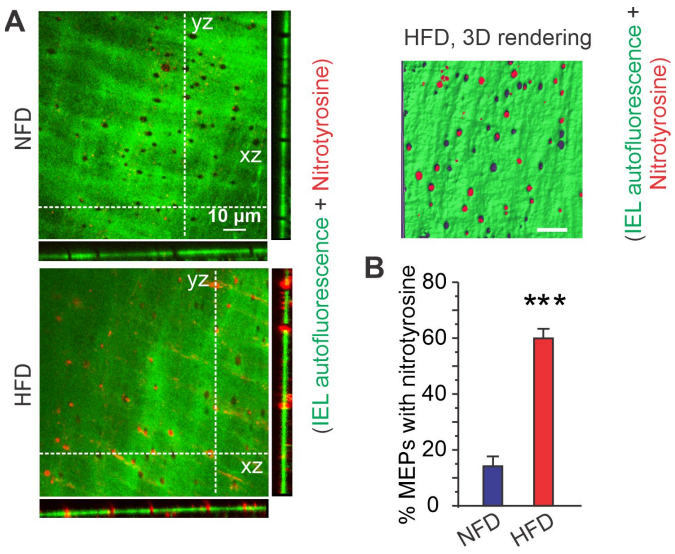

Supplemental Figure 14. (A) Representative 2D (*left*) and 3D (*top right*) merged z-stack images from *en face* preparations of third-order MAs showing IEL autofluorescence (green) and nitrotyrosine (NT) immunofluorescence (red) in NFD and HFD mice. Scale: 10 µm. (B) Quantification of NT localization at MEPs in NFD and HFD mice (n = 5; ***$P < 0.001$ for NFD vs. HFD; one-way ANOVA).

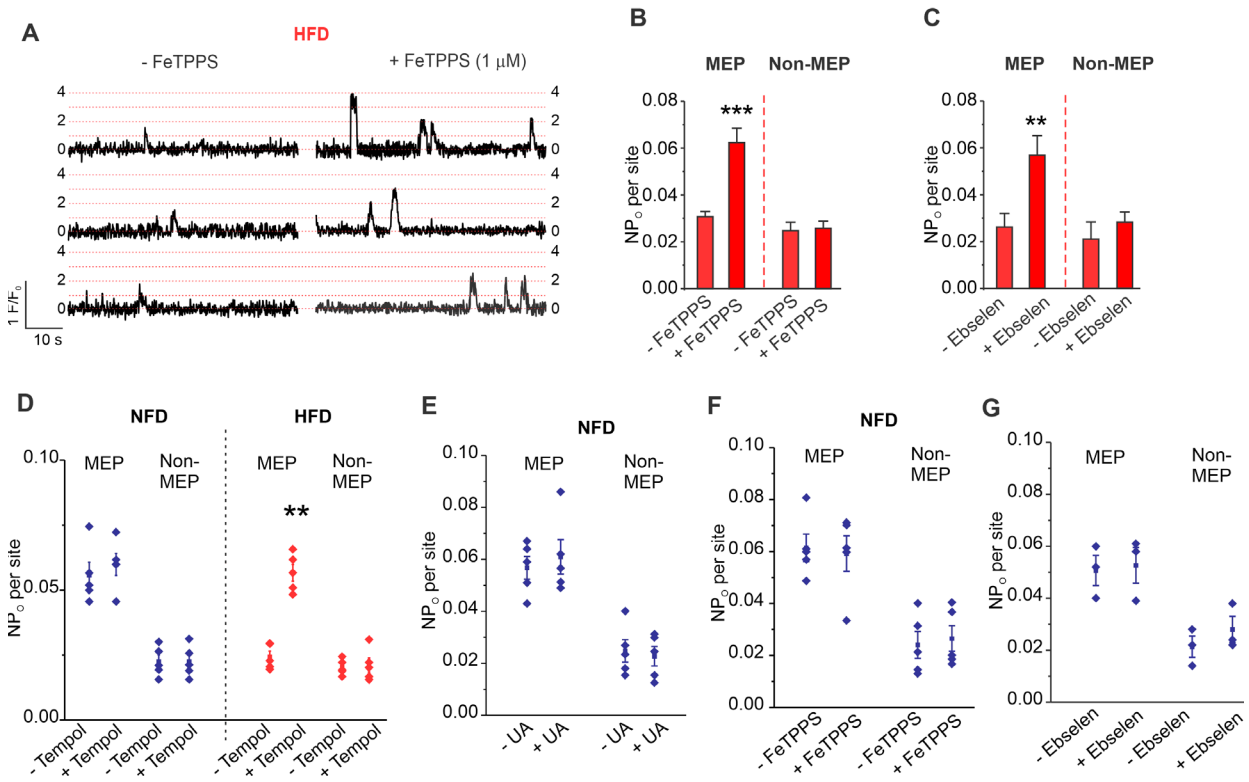

Supplemental Figure 15. Peroxynitrite inhibitors FeTPPS, Tempol, ebselen, and uric acid (UA) rescue TRPV4$_{EC}$ sparklet activity in mesenteric arteries (MAs) from obese (HFD) mice, but not in non-obese (NFD) mice. (A) Representative F/F$_0$ traces from TRPV4$_{EC}$ sparklet activity sites localized at the MEPs in fluo4-loaded MAs from HFD mice in the presence of GSK101 (3 nM, *left*) and GSK101+FeTPPS (1 μM, *right*). Dotted red lines indicate the quantal levels. (B) Averaged basal TRPV4$_{EC}$ sparklet activity (NP$_O$) at MEPs and non-MEP sites in MAs from HFD mice in the absence or presence of FeTTPS (1 μM, n=5 ***$P < 0.001$ vs. - FeTPPS, one-way ANOVA). (C) Averaged basal TRPV4$_{EC}$ sparklet activity at the MEPs and non-MEP sites in MAs from HFD mice in the absence or presence of Ebselen (1 μM, n=5, **$P < 0.01$ vs. - Ebselen, one-way ANOVA). (D) Averaged basal TRPV4$_{EC}$ sparklet activity at the MEPs and non-MEP sites in MAs from NFD (*left*) and HFD (*right*) mice in the absence or presence of Tempol (200 μM, n=5 **$P < 0.01$ vs. -Tempol, one-way ANOVA). (E) Averaged basal TRPV4$_{EC}$ sparklet activity at the MEPs and non-MEP sites in MAs from NFD mice in the absence or presence of Uric acid (200 μM, n=5). (F) Averaged basal TRPV4$_{EC}$ sparklet activity at the MEPs and non-MEP sites in MAs from NFD mice in the absence or presence of FeTTPS (1 μM, n=5). (G) Averaged basal TRPV4$_{EC}$ sparklet activity (NP$_O$) at MEPs and non-MEP sites in MAs from NFD mice in the absence or presence of ebselen (1 μM, n=3).

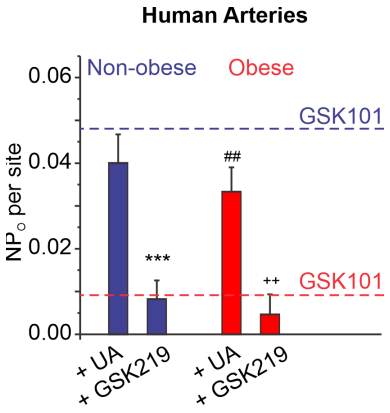

Supplemental Figure 16. PN inhibition rescues GSK219-sensitive TRPV4$_{EC}$ sparklet activity in obese patients. Averaged TRPV4$_{EC}$ sparklet activity (NP_O, 10 nM GSK101 present) in splenius and temporalis muscle arteries from non-obese and obese individuals in absence (dotted lines) or presence of Uric Acid (200 μM) (n=3-4; $^{\#\#}P < 0.01$ for arteries from obese patients with GSK101 + UA vs. GSK101 only; $^{++}P < 0.01$ for arteries from obese patients with UA + GSK101 vs. UA + GSK101 + GSK219; $^{**}P < 0.001$ for arteries from non-obese individuals, UA + GSK101 vs. UA + GSK101 + GSK219).

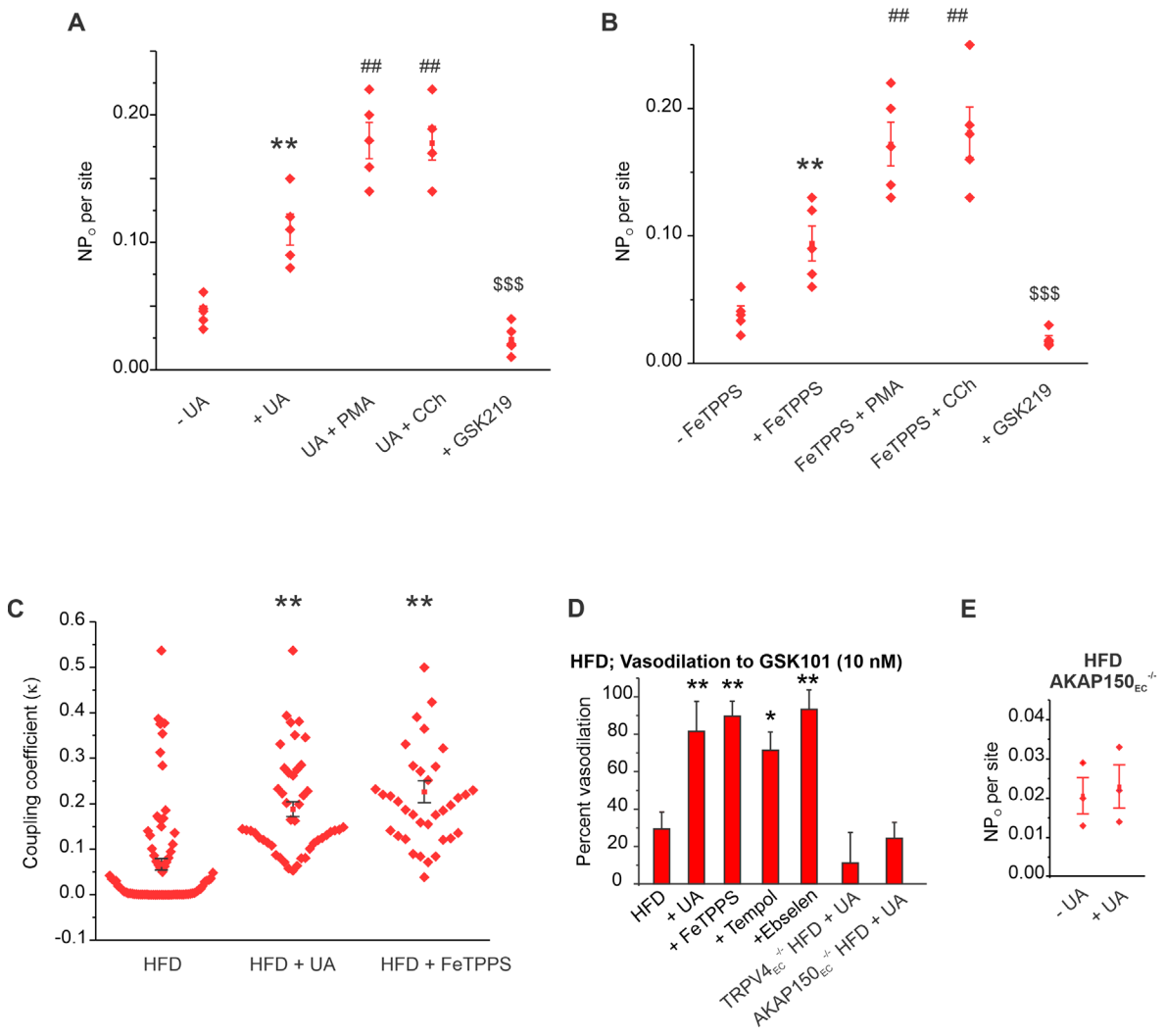

Supplemental Figure 17. Peroxynitrite inhibitors restore muscarinic receptor- and protein kinase C-activation of TRPV4$_{EC}$ sparklets, coupled gating of TRPV4 channels, and vasodilation to GSK101 in mesenteric arteries (MAs) from obese (HFD) mice. (A) Averaged TRPV4$_{EC}$ sparklet activity (NP_O) at MEPs in MAs from HFD mice in the absence or presence of Uric Acid (UA, 200 μM), Uric Acid+PMA (PKC activator, 10 nM), Uric Acid+Carbachol (muscarinic receptor agonist, 10 μM), and GSK219 (100 nM, $^{**}P < 0.01$ versus - UA, $^{\#\#}< 0.01$ versus + UA, $^{\$\$\$}<0.001$ versus UA+CCh, one-way ANOVA, n=4-5). (B) Averaged TRPV4$_{EC}$ sparklet activity (NP_O) at the MEPs in MAs from HFD mice in the absence or presence of FeTPPs (1 μM), FeTPPS+PMA (10 nM), FeTPPS+Carbachol (10 μM), and GSK219 (100 nM, $^{**}P < 0.01$ versus - FeTPPS, $^{\#\#}< 0.01$ versus + FeTPPS, $^{\$\$\$}< 0.001$ versus FeTPPS+CCh, one-way ANOVA, n=4-5). (C) Averaged coupling coefficient (κ) values for TRPV4$_{EC}$ sparklet sites at MEP locations in MAs from HFD mice in the absence or presence of Uric Acid or FeTPPS (n=36-72, $^{**}P < 0.01$ versus HFD, one-way ANOVA). κ values vary from 0 (no coupling or independent gating) to 1 (maximum coupling). (D) Averaged diameter data for GSK101 (10 nM)-

induced dilation of MAs from HFD, HFD $TRPV4_{EC}^{-/-}$, and HFD $AKAP150_{EC}^{-/-}$ mice at baseline, in presence of Uric Acid, FeTTPS, Tempol, and Ebselen (n=5; $^{**}P < 0.01$ versus HFD). (E) $TRPV4_{EC}$ sparklet activity before and after the addition of uric acid (UA, 200 μM) in HFD $AKAP150_{EC}^{-/-}$ (n=3).

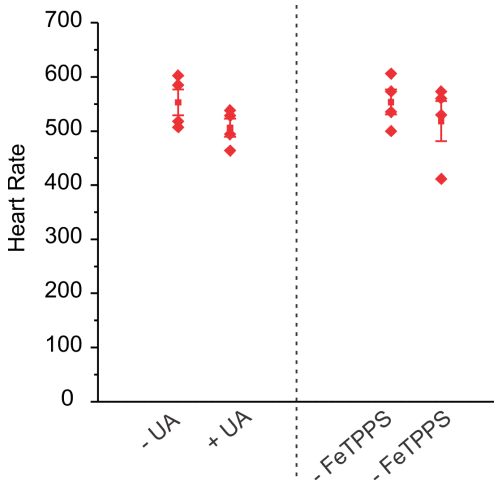

Supplemental Figure 18. Peroxynitrite inhibitors do not alter the heart rate in obese mice. Averaged heart rate of HFD mice before and 15 minutes after intraperitoneal injection of Uric Acid (UA, 200 mg/kg) or FeTPPS (10 mg/kg), n=4.

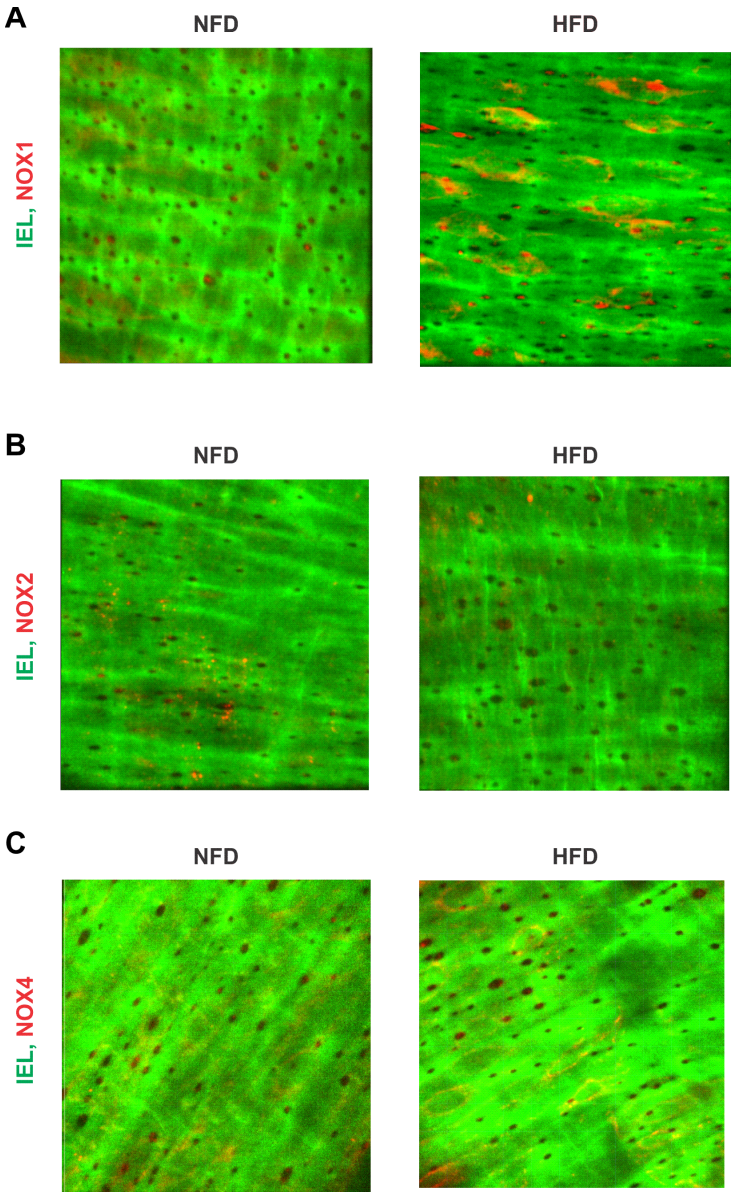

Supplemental Figure 19. Diet-induced obesity increases the expression of NOX1, but not NOX2 and NOX4, at the MEPs in mesenteric arteries (MAs). (A) Representative merge images from *en face* third-order MAs showing internal elastic lamina (IEL) autofluorescence (green) and NOX1 immunostaining (red) in normal (NFD, *left*) and obese (HFD, *right*) mice. (B) Representative merge images from *en face* third-order MAs showing internal elastic lamina (IEL) autofluorescence (green) and NOX2 immunostaining (red) in NFD (*left*) and HFD (*right*) mice. (C) Representative merge images from *en face* third-order MAs showing internal elastic lamina (IEL) autofluorescence (green) and NOX4 immunostaining (red) in NFD (*left*) and HFD (*right*) mice.

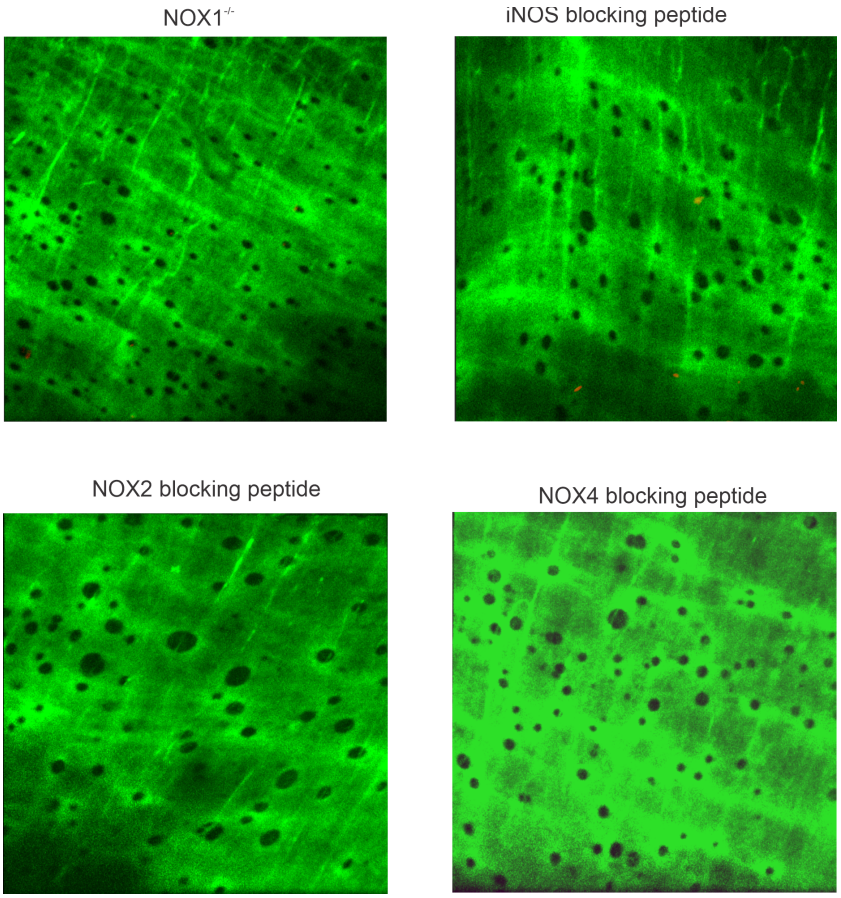

Supplemental Figure 20. Validation of NOX1/2/4 and iNOS antibodies. Representative merge images of *en face* third-order MAs from NOX1$^{-/-}$ mouse (*top-left*), and from WT mice showing internal elastic lamina (IEL) autofluorescence (green); black holes represent the MEPs. *Top panel*, *left*, NOX1 immunostaining (red) in arteries from NOX1$^{-/-}$ mice; *Top panel*, *right*, iNOS immunostaining after pre-treating the iNOS antibody with blocking peptide (antibody epitope); *bottom panel*, *left*, NOX2 immunostaining after pre-treating the NOX2 antibody with the blocking peptide; *bottom panel*, *right*, NOX4 immunostaining after pre-treating the NOX4 antibody with blocking peptide.

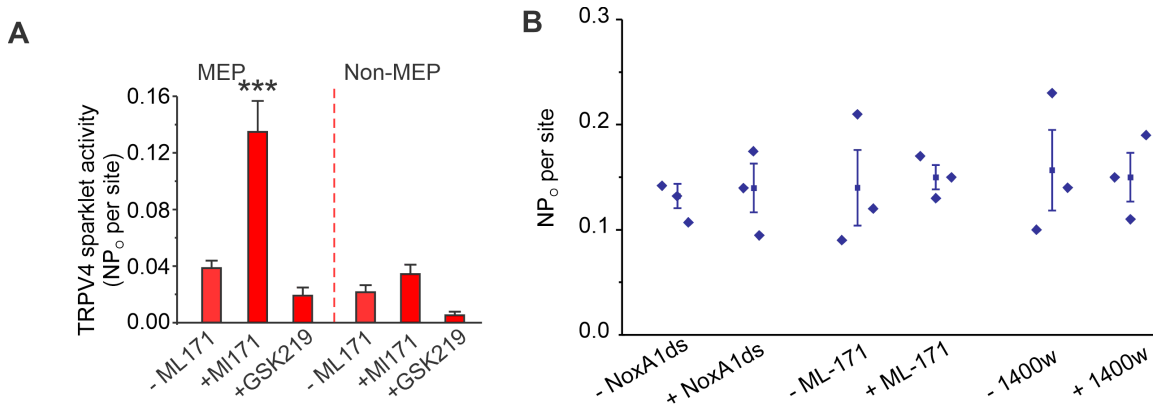

Supplemental Figure 21. NOX1 inhibition improves TRPV4$_{EC}$ activity in obese mice, but not in non-obese mice. (A) Averaged TRPV4$_{EC}$ sparklet activity (GSK101, 10 nM) at MEPs in MAs from HFD mice in the absence or presence of the ML-171 (1 μM, n = 5; ***P < 0.001 vs. -ML171; one-way ANOVA). (B) Averaged TRPV4$_{EC}$ sparklet activity (10 nM GSK101) at MEPs in mesenteric arteries (MAs) from NFD mice in the absence or presence of NOX1 inhibitors, NoxA1ds and ML-171 (1 μM, n=3), or iNOS inhibitor, 1400w (1 μM, n=3).

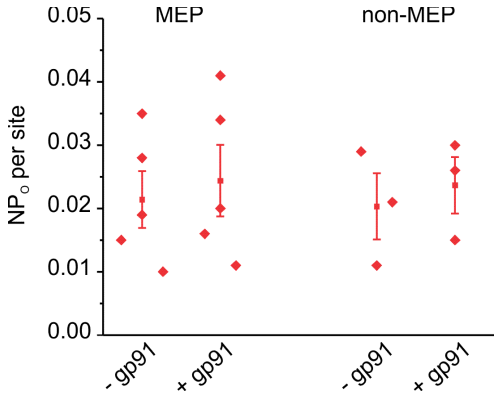

Supplemental Figure 22. NOX2 inhibition does not restore TRPV4$_{EC}$ sparklet activity in obese (HFD) mice. Averaged TRPV4$_{EC}$ sparklet activity (NP_O) in mesenteric arteries (MAs) from HFD mice in the absence or presence of gp91 ds-tat (gp91, 1 μM, n=3-5).

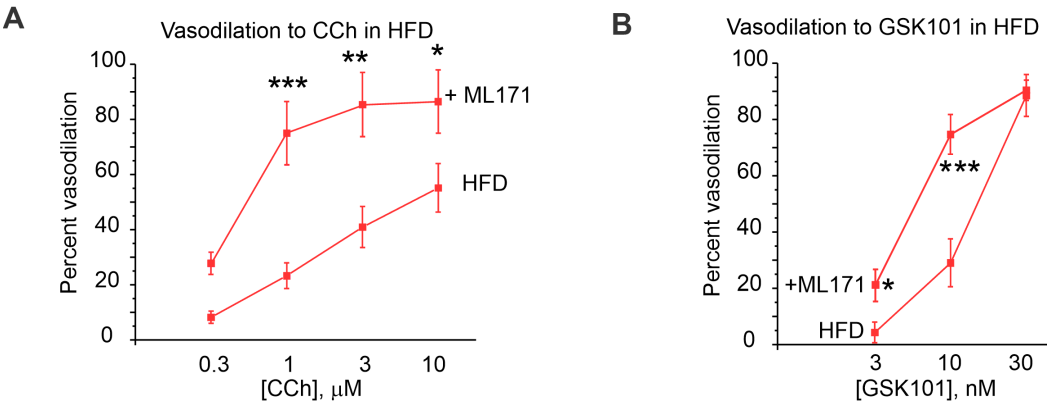

Supplemental Figure 23. NOX1 inhibition rescues endothelium-dependent vasodilation in HFD mice. (A) Effects of ML-171 on CCh (0.3–10 μM)-induced dilation of MAs from HFD mice (n = 5–8; ***$P < 0.001$ [1 μM CCh], **< 0.01 [3 μM CCh] and *< 0.05 [10 μM CCh] for ML171-treated HFD vs. HFD only; two-way ANOVA). (B) Effects of ML-171 on GSK101 (3–10 nM)-induced dilation of MAs from HFD mice (n = 5–9; ML171: **$P < 0.01$ [3 nM GSK101] and ***< 0.001 [10 nM GSK101] for ML171-treated HFD vs. HFD only; two-way ANOVA).

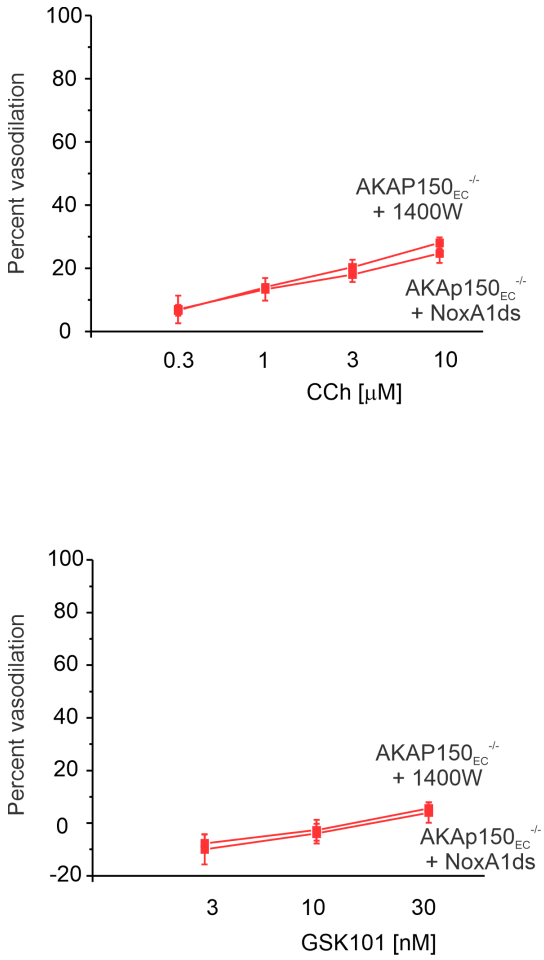

Supplemental Figure 24. NOX1 or iNOS inhibitors do not rescue endothelium-dependent vasodilation in obese AKAP150$_{EC}^{-/-}$ mice. The effect of iNOS inhibitor 1400W (1 μM) and NOX1 inhibitor NoxA1ds (1 μM) on vasodilation to CCh (*top*) or GSK101 (*bottom*) in HFD AKAP150$_{EC}^{-/-}$ mice (n=3).

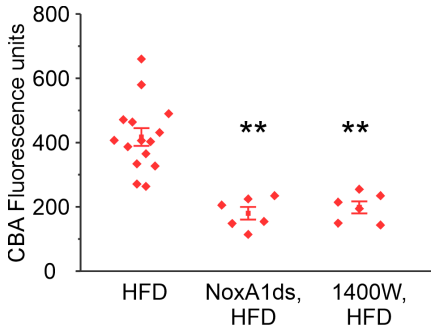

Supplemental Figure 25. NOX1 or iNOS inhibition reduce PN formation in HFD mice. Averaged coumarin boronic acid (CBA) fluorescence intensity in ECs of MAs from HFD mice at baseline and in the presence of NoxA1ds or 1400W (n=6-16 fields, $^{**}P<0.01$ for NoxA1ds and 1400W vs. HFD only; one-way ANOVA).

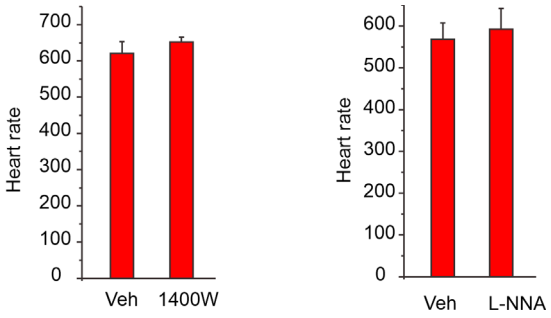

Supplemental Figure 26. iNOS or NOS inhibition lowers mean arterial pressure (MAP) in obese mice. Quantification of heart rate (per minute) in HFD mice following i.p. injection of 1400W (10 mg/kg) or L-NNA (100 mg/kg) compared to HFD mice treated with vehicle [Veh, saline], n=3-5.

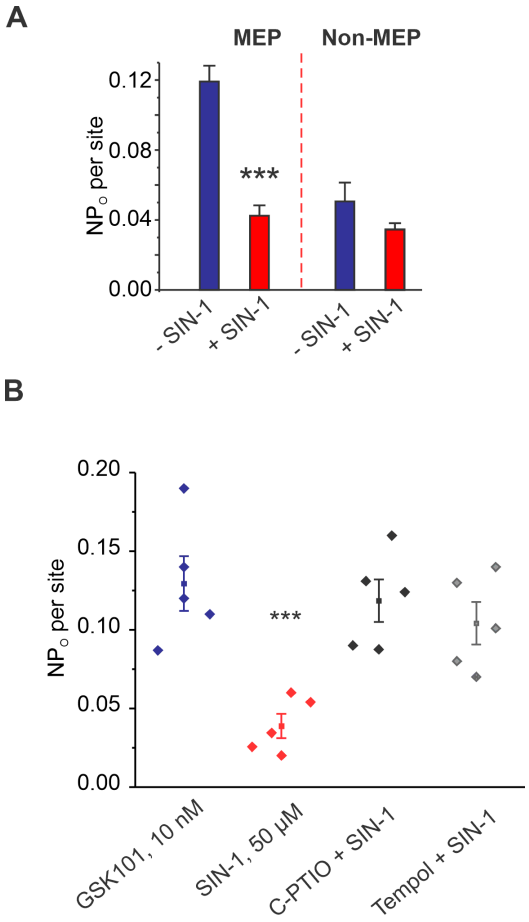

Supplemental Figure 27. Exogenous PN, not superoxide or nitric oxide (NO), impairs TRPV4$_{EC}$ channel activity. (A) Averaged GSK101 (10 nM)-stimulated-TRPV4$_{EC}$ sparklet activity (NP_O) at MEP and non-MEP sites in MAs from WT mice in the absence or presence of the PN donor SIN-1 (50 μM) (n = 5; ***$P < 0.001$ for NP_O at MEP sites in the presence vs. absence of SIN-1; one-way ANOVA). (B) Averaged GSK101 (10 nM)-stimulated TRPV4$_{EC}$ sparklet activity (NP_O) at the MEPs in MAs from NFD mice after SIN-1 (50 μM) application in the pretreatment of NO scavenger carboxy-PTIO (C-PTIO, 50 μM) or Tempol (200 μM) (n=5, ***$P < 0.001$ SIN-1 versus GSK101, one-way ANOVA.

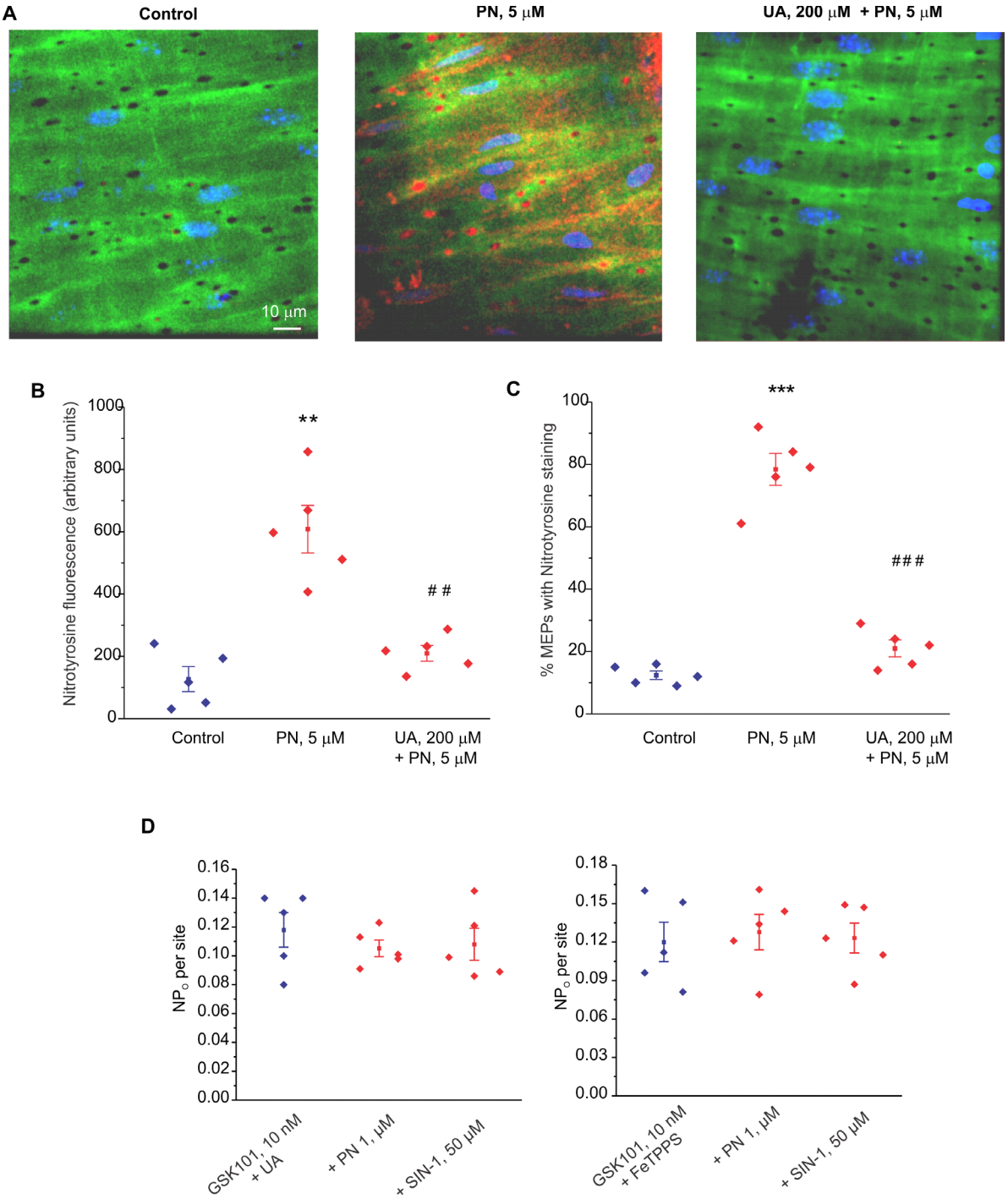

Supplemental Figure 28. Peroxynitrite (PN)-induced increase in nitrotyrosine formation and a decrease in TRPV4 sparklet activity are prevented by a PN inhibitors. (A) Representative merge images from *en face* third-order MAs of normal (NFD) mice showing internal elastic lamina (IEL) autofluorescence (green), endothelial cells nuclei (blue), and nitrotyrosine staining (red) under basal condition (*left*, Control) or after PN (5 μM) application in

the absence (*middle*) or presence of Uric Acid (UA, 200 μM, *right*). (B) Quantification of global nitrotyrosine staining from *en face* third-order MAs from NFD mice under basal condition or after PN (5 μM) application in the absence or presence of UA (n=5, $^{**}P < 0.01$ versus Control, $^{\#\#}P < 0.01$ versus PN, one-way ANOVA). (C) Percentage of nitrotyrosine staining at the MEPs in MAs from NFD mice under basal condition or after PN (5 μM) application in the absence or presence of UA (200 μM, n=5, $^{***}P < 0.001$ versus Control, $^{\#\#\#}P < 0.001$ versus PN, one-way ANOVA). (D) Averaged GSK101 (10 nM)-stimulated $TRPV4_{EC}$ sparklet activity (NP_O) at the MEPs in MAs from NFD mice following PN (1 μM) or SIN-1 (1 μM) in the MAs pretreated with UA (*left*) or FeTPPS (1 μM, *right*), n=5.

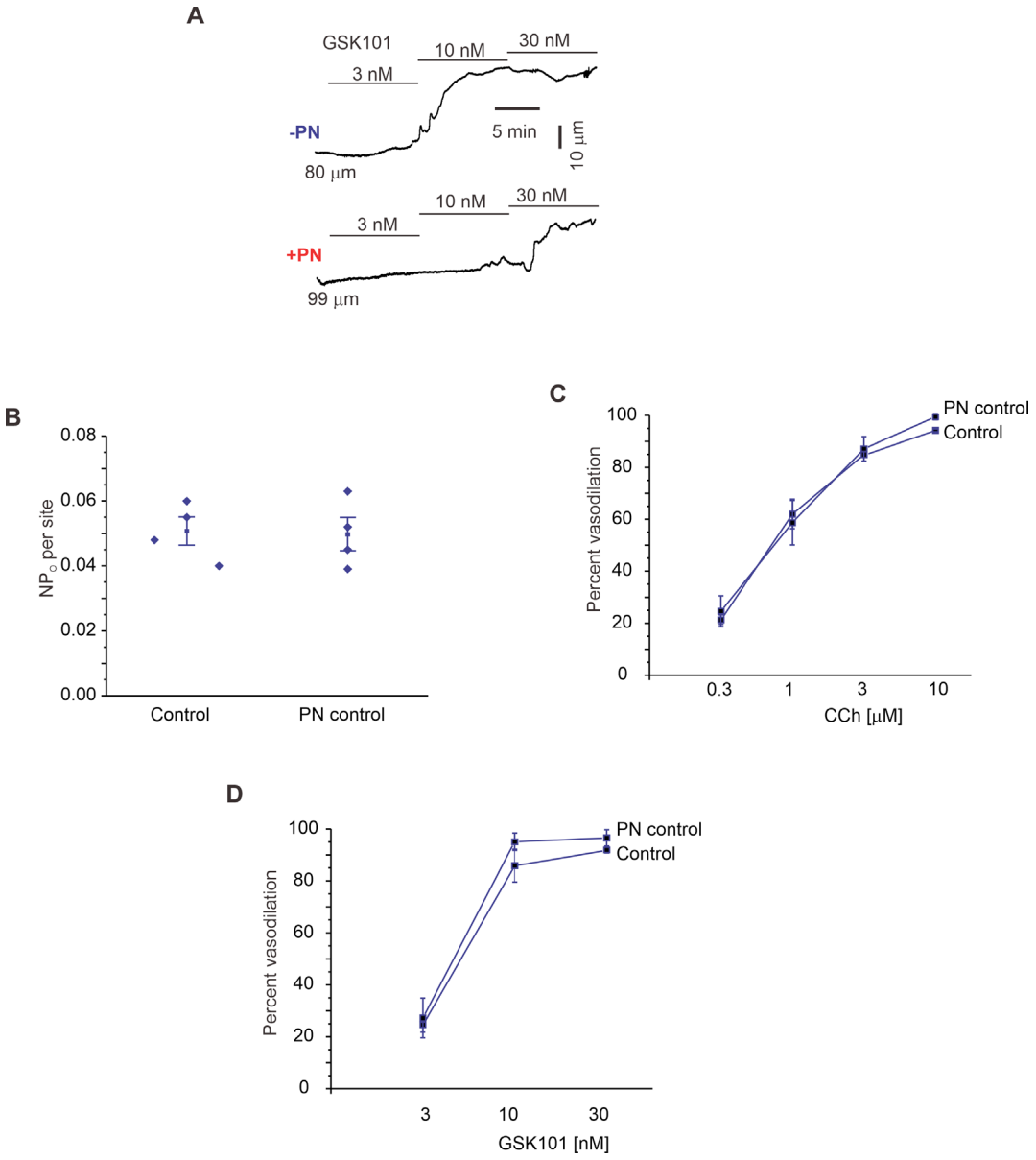

Supplemental Figure 29. Peroxynitrite (PN) lowers endothelium-dependent vasodilation, while decomposed peroxynitrite has no effect on TRPV4$_{EC}$ sparklet activity or vasodilation. (A) Representative diameter traces for vasodilation to GSK101 (3–30 nM) in MAs from non-obese mice in the absence or presence of PN. (B) The effect of decomposed PN on GSK101 (3 nM)-stimulated TRPV4$_{EC}$ sparklet activity (n=4) in ECs of *en face* MAs from non-obese mice. (C) The effect of decomposed PN on vasodilation to CCh (n=3) in MAs from non-obese mice. (D) The effect of decomposed PN on vasodilation to GSK101 (n=3) in MAs from non-obese mice.

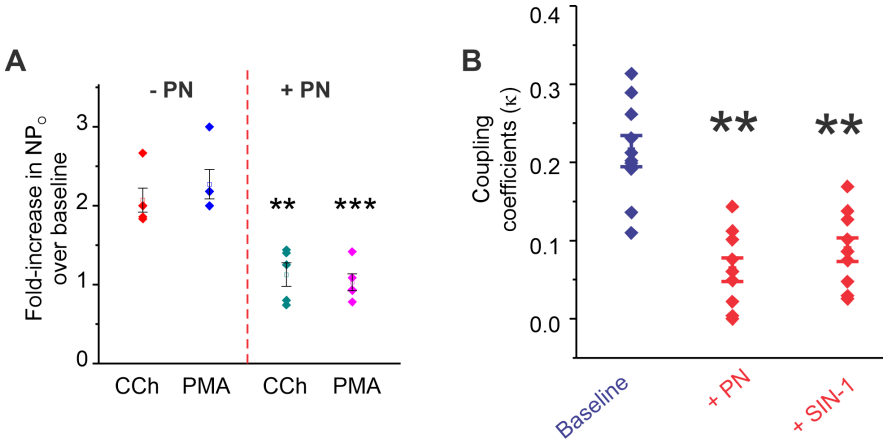

Supplemental Figure 30. Peroxynitrite (PN) impairs muscarinic receptor and protein kinase C (PKC) activation of, and coupling strength amongst TRPV4$_{EC}$ channels. (A) Scatter plot showing CCh- and PMA-induced increases in TRPV4$_{EC}$ sparklet activity (NP_O) at MEP sites relative to baseline (20 μM CPA), in the absence or presence of PN, in MAs from WT mice (n = 5; $^{**}P < 0.01$ for CCh-treated vs. baseline, $^{***}P < 0.001$ for PMA-treated vs. baseline; one-way ANOVA). (B) The effect of PN and SIN-1 on coupling coefficients among TRPV4$_{EC}$ sparklets (n=9-10; $^{**}P<0.01$ vs. baseline; one-way ANOVA).

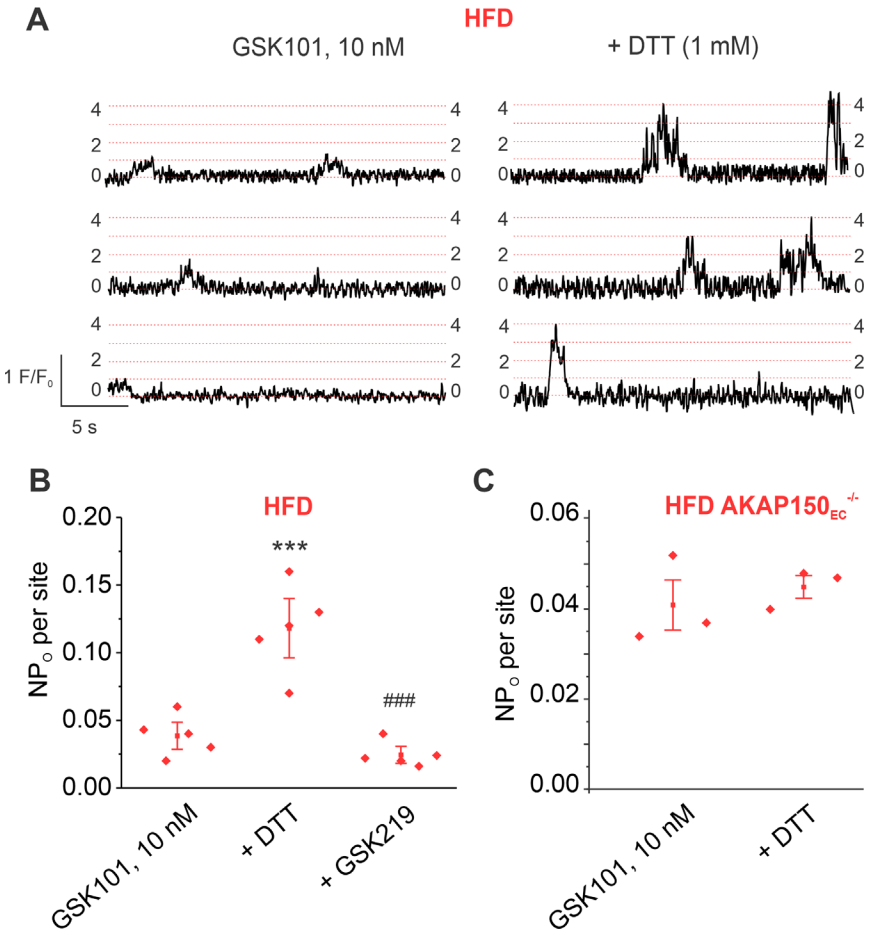

Supplemental Figure 31. Reversing cysteine oxidation via dithiothreitol (DTT) rescues endothelial TPRV4 sparklet activity in a AKAP150$_{EC}$-dependent manner. (A) Representative baseline F/F$_0$ traces from TRPV4$_{EC}$ sparklet sites localized at the MEPs in fluo4-loaded MAs from HFD mice in presence of GSK101 (10 nM, *left*) and GSK101+DTT (1 mM, *right*). Dotted red lines indicate the quantal levels (i.e. stepwise openings of 1–4 TRPV4$_{EC}$ channels at a site). (B) Averaged TRPV4$_{EC}$ sparklet activity (NP$_O$) at the MEPs in MAs from HFD mice in the presence of GSK101 (10 nM), GSK101+DTT (1 mM), and GSK101+DTT+GSK219 (100 nM, data are mean ± SEM, n=5, $^{***}P < 0.001$ versus GSK101; $^{###}P < 0.001$ versus DTT, one-way ANOVA). (C) TRPV4$_{EC}$ sparklet activity in obese AKAP150$_{EC}^{-/-}$ mice before and after addition of DTT (n=3).

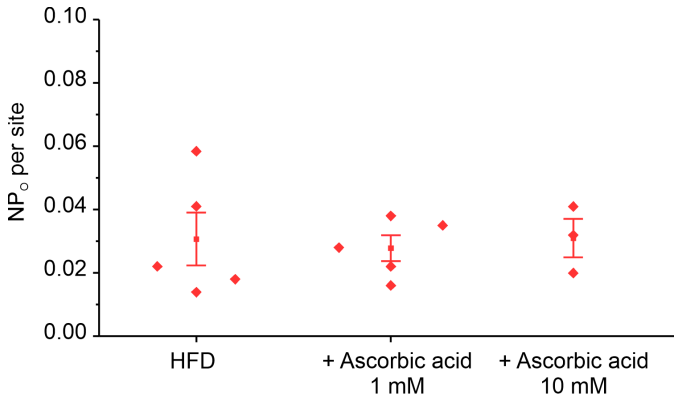

Supplemental Figure 32. Denitrosylating agent ascorbic acid does not rescue $TRPV4_{EC}$ sparklet activity in obesity. $TRPV4_{EC}$ sparklet activity (NP_O) in MAs from HFD mice in the presence of GSK101 (3 nM), and GSK101+Ascorbic Acid (1-10 mM), n=3-5.

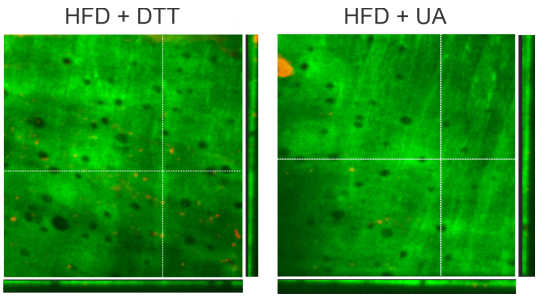

Supplemental Figure 33. Reducing disulfide bonds and scavenging PN lowers cysteine sulfenic acid (CSA) formation at MEPs. Representative merge images of cysteine sulfenic acid staining in *en face* third-order MAs from HFD mice pre-treated with Dithiothreitol (DTT) (*left*) or Uric Acid (UA) (*right*) showing internal elastic lamina (IEL) autofluorescence (green) and CSA staining (red).

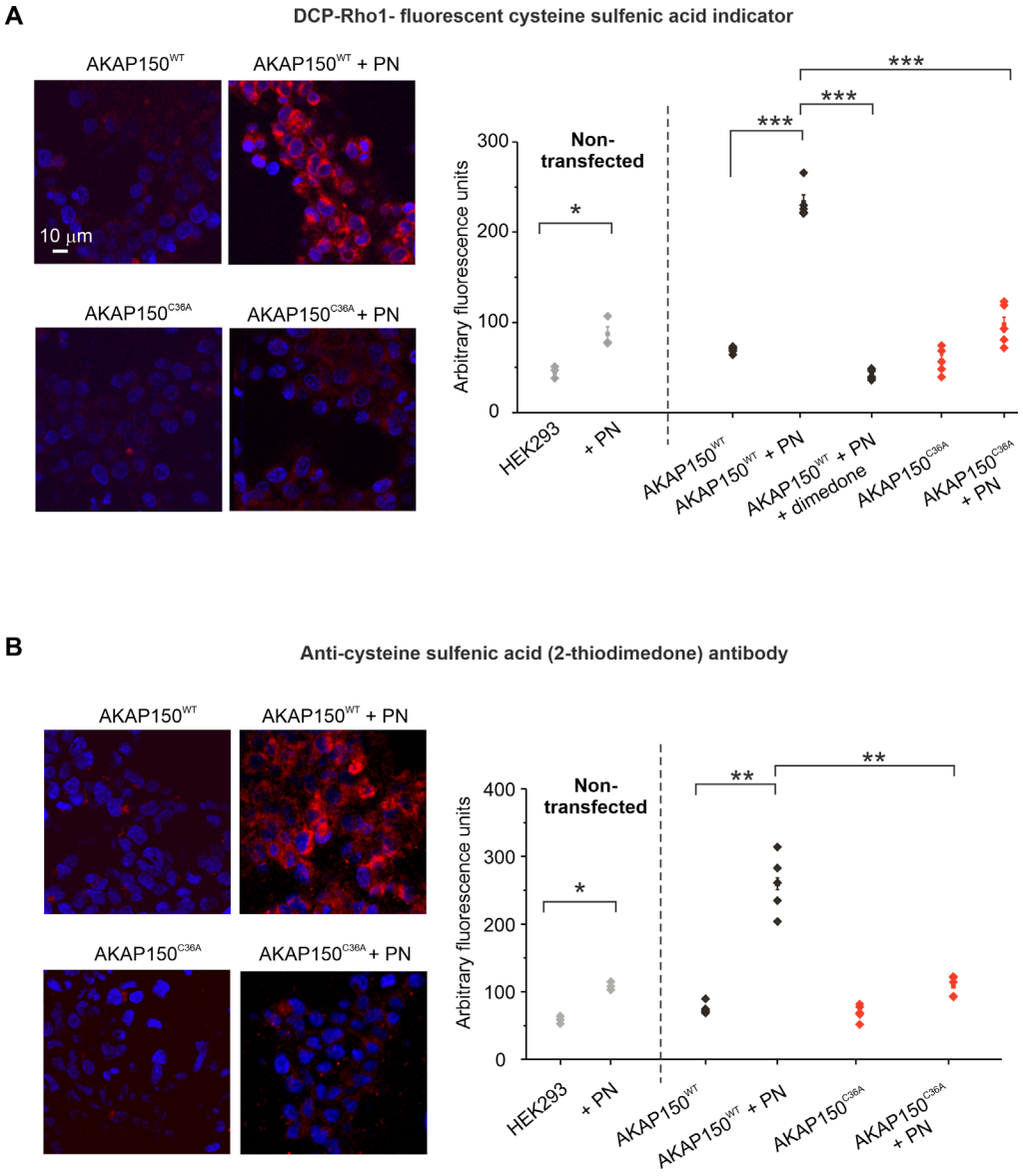

Supplemental Figure 34. PN causes Cysteine36 oxidation of AKAP150. (A) *Left*, representative images of HEK293 cells transfected with wild-type AKAP150 ($AKAP150^{WT}$) (*top*) and AKAP150 (Cys36 to Ala or $AKAP150^{C36A}$) (*bottom*) and treated with DCP-Rho1 (1 μM), a fluorescent indicator of cysteine sulfenic acid, in presence or absence of PN (10 μM), nuclei were stained with DAPI; *right*, averaged mean fluorescence intensity per cell for DCP-Rho1 in non-transfected and transfected HEK293 cells. Regions of interest were drawn around each cell to determine the mean fluorescence intensity, and mean fluorescence intensity for each group was averaged across each experiment (n=3-5, * $P<0.05$ for non-transfected HEK293 cells vs. non-transfected HEK293 cells + PN, *** $P<0.001$ $AKAP150^{WT}$ vs. $AKAP150^{WT}$ + PN; *** $P<0.001$ $AKAP150^{WT}$ + PN vs. $AKAP150^{WT}$ + PN + dimedone). Dimedone treatment prior to DCP-Rho1 addition abolished PN-induced increase in DCP-Rho1 fluorescence. (B) *Left*, representative images for cysteine sulfenic acid staining in HEK293 cells transfected with $AKAP150^{WT}$ (*top*) or $AKAP150^{C36A}$ (*bottom*), nuclei were stained

with DAPI; *right*, scatter plot of averaged cysteine sulfenic acid fluorescence in non-transfected and transfected HEK293 cells (n=3-5, * $P<0.05$ for non-transfected HEK293 cells vs. non-transfected HEK293 cells + PN, *** $P<0.001$ $AKAP150^{WT}$ vs. $AKAP150^{WT}$ + PN). (D) 2-thiodimedone staining in non-transfected HEK293 cells with or without PN (n=3, * $P<0.05$; t-test).

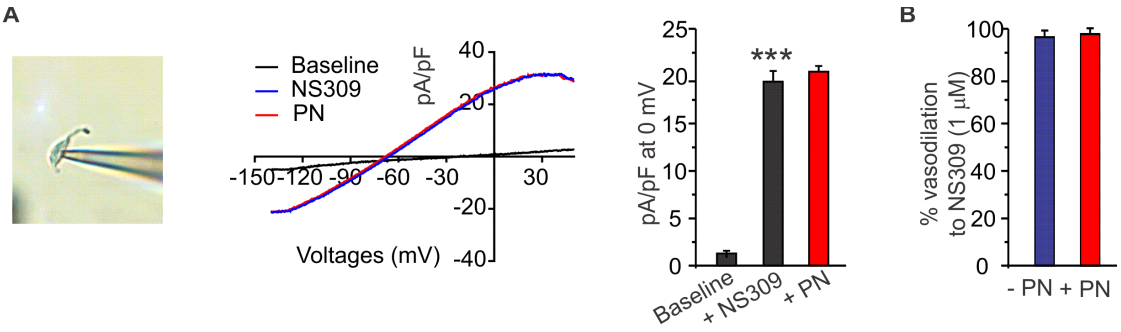

Supplemental Figure 35. Peroxynitrite (PN) does not inhibit currents through endothelial IK/SK channels. (A) Freshly isolated endothelial cell from MAs in a perforated patch clamped configuration (*left*). Representative traces (*middle*) and current density plot (*right*) of endothelial IK/SK currents under baseline conditions and in the presence of NS309 (1 µM) or NS309 + PN (5 µM) (n = 6; ***$P < 0.001$ for baseline versus NS309; one-way ANOVA). (B) Averaged diameter data for NS309-induced dilations of MAs from NFD mice in the presence or absence of PN (n = 5).

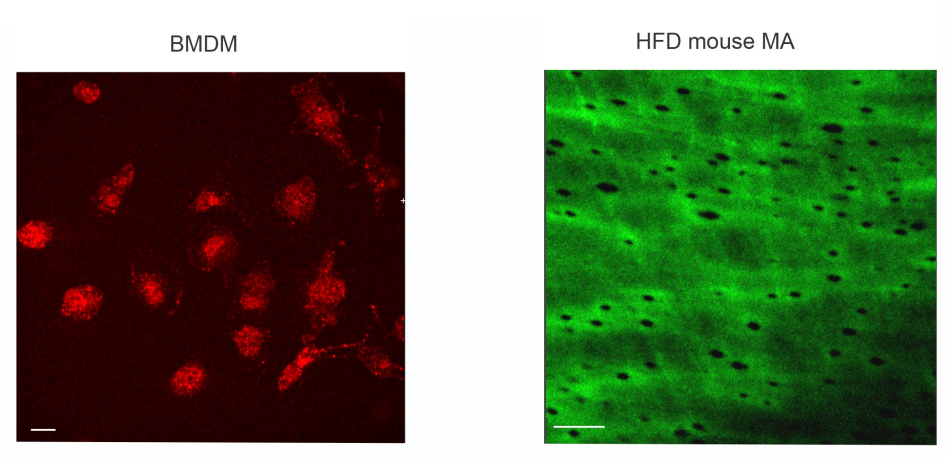

Supplemental Figure 36. Arteries from obese mice do not show CD45 staining in the IEL. Anti-CD45 staining (red) in mouse bone-marrow derived macrophages (BMDM, *left*) and *en face* mesenteric artery (MA) from a HFD mouse (*left*). Green color indicates IEL autofluorescence. Scale bar: 20 μm.

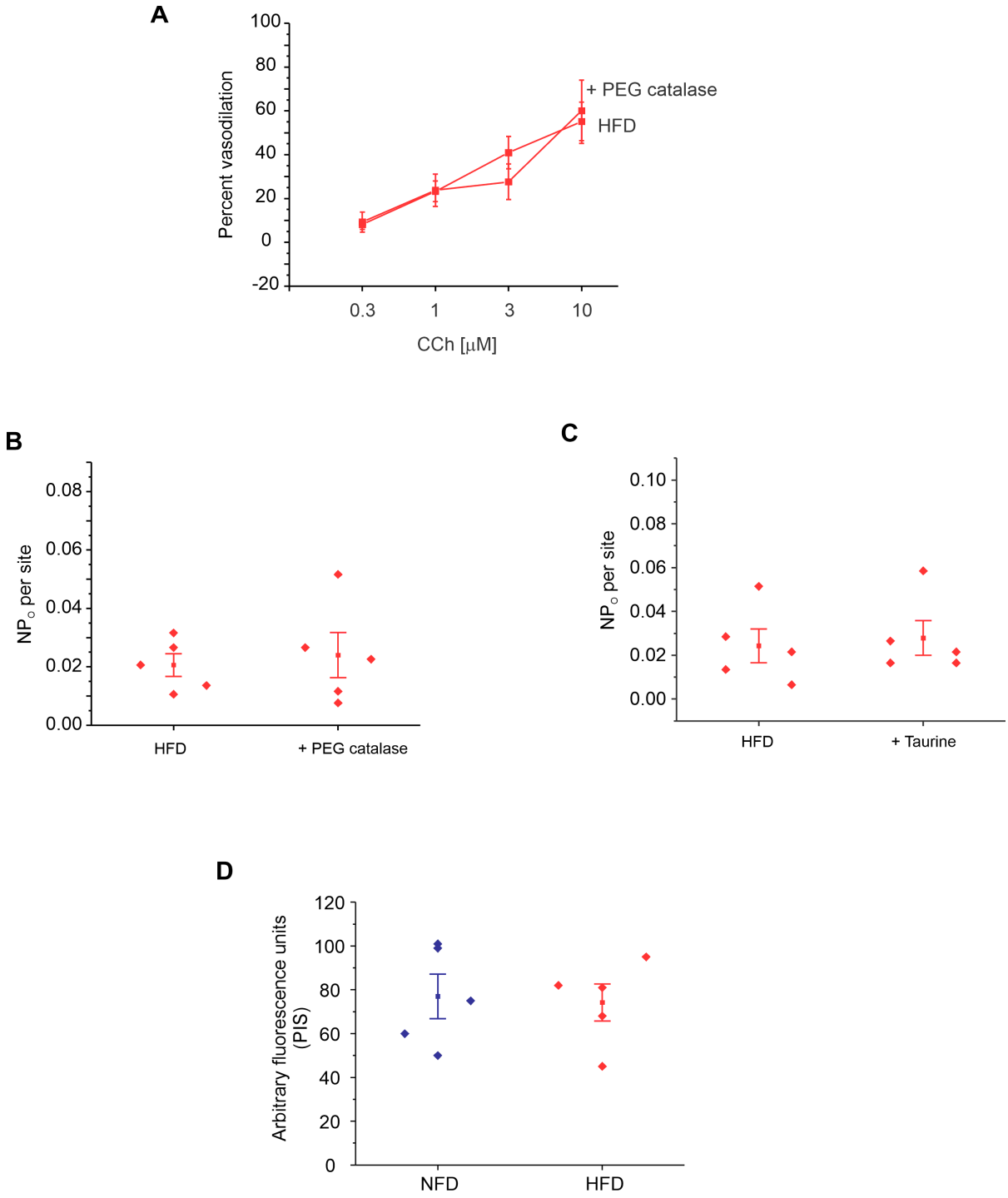

Supplemental Figure 37. Hydrogen peroxide and hypochlorous acid inhibition do not rescue TRPV4$_{EC}$ channel activity and endothelium-dependent vasodilatation in obesity. (A) Effects of PEG-catalase (500 U/mL) on CCh (0.3–10 μM)-induced dilation of MAs from HFD mice (n = 5). (B) Averaged TRPV4$_{EC}$ sparklet activity (NP_O) (GSK101, 3 nM) in MAs from HFD mice in the absence or presence of PEG-catalase (500 U/mL), n=5. (C) Averaged TRPV4$_{EC}$ sparklet activity (NP_O) (GSK101, 3 nM) in MAs from HFD mice in the absence or presence of

Taurine (1 mM), n=5. (D) Arbitrary fluorescence intensity of hypochlorite probe PIS in endothelial cells from NFD and HFD mice (n=5).

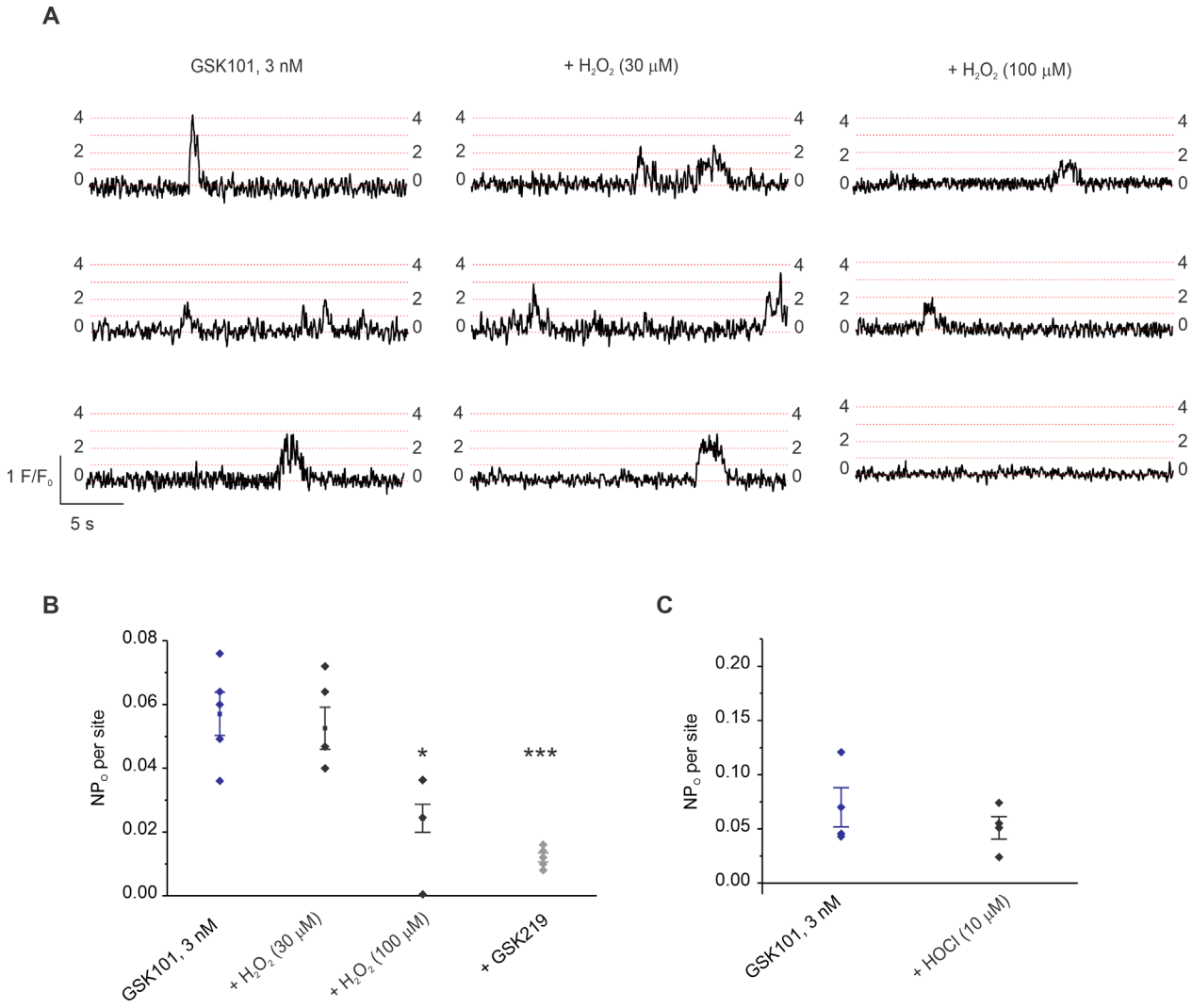

Supplemental Figure 38. Hydrogen peroxide and hypochlorous acid do not impair TRPV4$_{EC}$ sparklet activity. (A) Representative baseline F/F_0 traces from TRPV4$_{EC}$ sparklet sites localized at the MEPs in fluo4-loaded MAs from NFD mice in the presence of GSK101 (3 nM, *left*), GSK101+H_2O_2 (30 μM, *middle*), and GSK101+H_2O_2 (100 μM, *right*). Dotted red lines indicate the quantal levels (i.e. stepwise openings of 1–4 TRPV4$_{EC}$ channels at a site). (B) Averaged TRPV4$_{EC}$ sparklet activity (NP_O) at the MEPs in MAs from NFD mice in the presence of GSK101 (3 nM), GSK101+H_2O_2 (30 μM), GSK101+H_2O_2 (100 μM), and GSK101+H_2O_2 (30 μM and 100 μM) +GSK219 (n=5, **P* < 0.5 GSK101 only vs. GSK101+H_2O_2 (100 μM); ****P*=0.001 GSK101 only vs. GSK101+H_2O_2 (30 μM and 100 μM) +GSK219, one-way ANOVA). (C) Averaged TRPV4$_{EC}$ sparklet activity (NP_O) at MEPs in MAs from NFD mice in the presence of GSK101 (3 nM) and GSK101+HOCl (10 μM), n=3.

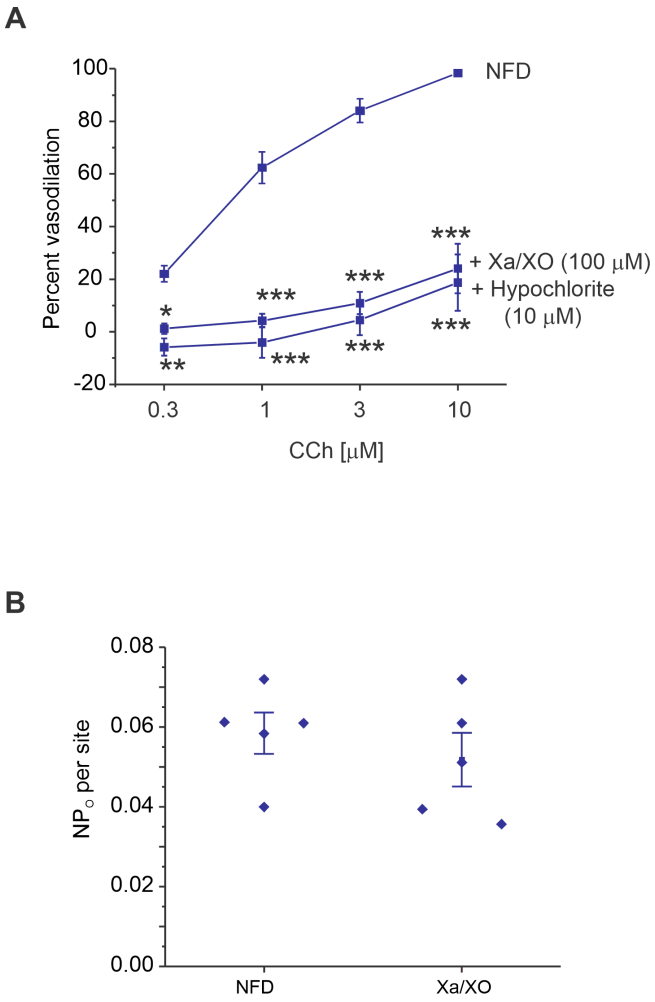

Supplemental Figure 39. Superoxide radicals and hypochlorous acid (HOCl) lower vasodilation but do not alter TRPV4$_{EC}$ sparklet activity. (A) Effects of Hypoxanthine (Xa, 100 μM)/Xanthine Oxidase (XO, 0.5 mU/mL) superoxide radical generating system and hypochlorite (10 μM) on CCh (0.3–10 μM)-induced dilation of MAs from NFD mice, n=5 *P < 0.05, **< 0.01, ***< 0.001 vs. NFD. (B) Averaged TRPV4$_{EC}$ sparklet activity (NP_O) (GSK101, 3 nM) in MAs from NFD mice in the absence or presence of Xa (100 μM)/XO (0.5 mU/mL), n=4-5.

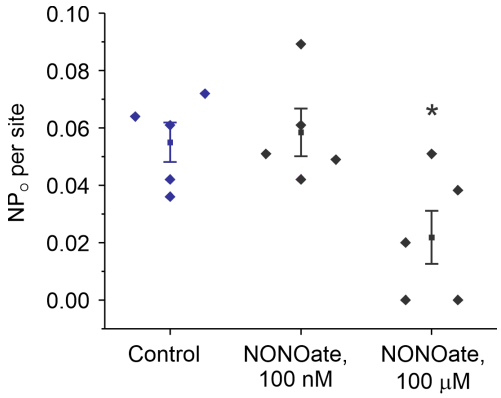

Supplemental Figure 40. NO donor spermine NONOate lowers TRPV4$_{EC}$ sparklet activity only at a high concentration. Averaged TRPV4$_{EC}$ sparklet activity (NP_O) in MAs from non-obese mice in the presence of GSK101 (3 nM) before and after the addition of spermine NONOate (100 nM and 100 μM), n=5; **P* < 0.05 vs. Control.

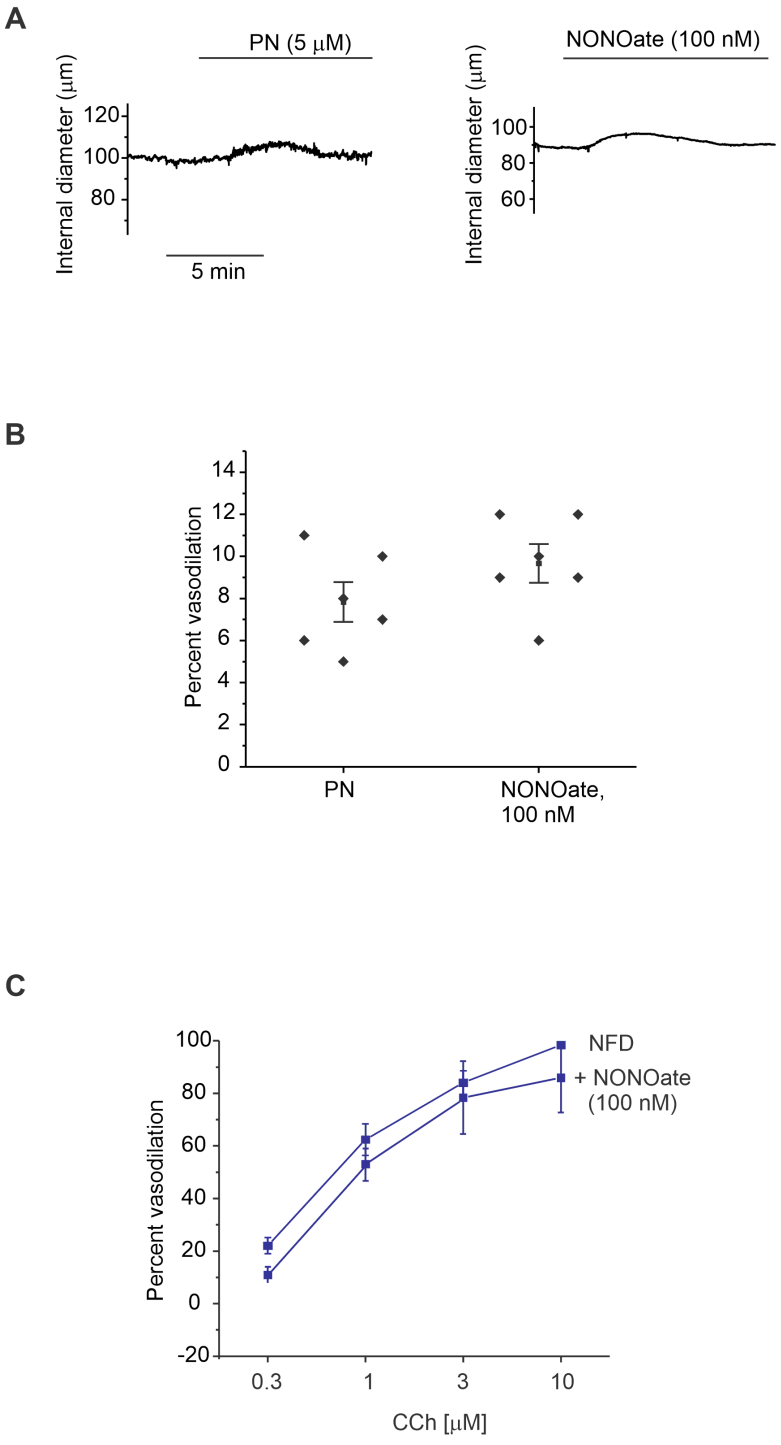

Supplemental Figure 41. Low concentration of peroxynitrite (PN) and NO donor cause a small vasodilation, and the NO donor does not alter CCh vasodilation. (A) Representative diameter traces of MAs from NFD mice treated with PN (5 μM) (*left*) or with spermine NONOate (100 nM) (*right*). (B) Averaged vasodilation of MAs from NFD mice in the presence of PN (5 μM) or NONOate (100 nM), n=6. (C) Effect of spermine NONOate (100 nM) on CCh (0.3-10 μM)-induced vasodilation, n=5.

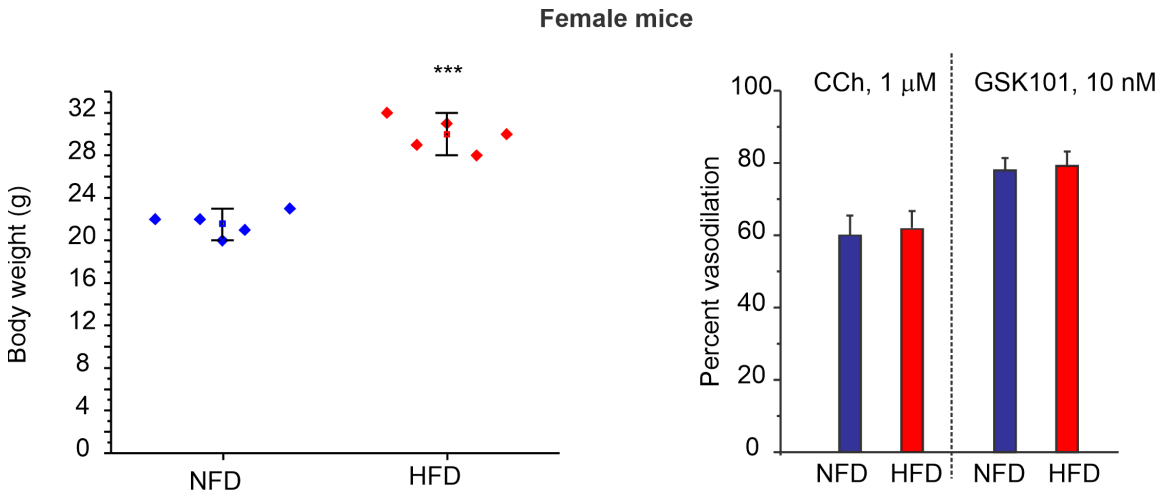

Supplemental Figure 42. High fat diet feeding for 14 weeks does not impair endothelium-dependent vasodilation in female mice. Averaged data showing body weight of female mice (*left*) fed with NFD and HFD for 14 weeks, starting at 6 weeks of age (n=5, ***P<0.001 NFD vs. HFD; one-way ANOVA). Averaged diameter data (*right*) for MAs from NFD and HFD female mice in response to CCh (1 μM) and to GSK101 (10 nM), n=5.

SUPPLEMENTAL REFERENCES

1. Moore C, Cevikbas F, Pasolli HA, Chen Y, Kong W, Kempkes C, Parekh P, Lee SH, Kontchou NA, Yeh I, Jokerst NM, Fuchs E, Steinhoff M and Liedtke WB. UVB radiation generates sunburn pain and affects skin by activating epidermal TRPV4 ion channels and triggering endothelin-1 signaling. *Proc Natl Acad Sci U S A*. 2013;110:E3225-34.
2. Sorensen I, Adams RH and Gossler A. DLL1-mediated Notch activation regulates endothelial identity in mouse fetal arteries. *Blood*. 2009;113:5680-8.
3. Biwer LA, Good ME, Hong K, Patel RK, Agrawal N, Looft-Wilson R, Sonkusare SK and Isakson BE. Non-Endoplasmic Reticulum-Based Calr (Calreticulin) Can Coordinate Heterocellular Calcium Signaling and Vascular Function. *Arterioscler Thromb Vasc Biol*. 2017.
4. Hong K, Cope EL, DeLalio LJ, Marziano C, Isakson BE and Sonkusare SK. TRPV4 (Transient Receptor Potential Vanilloid 4) Channel-Dependent Negative Feedback Mechanism Regulates Gq Protein-Coupled Receptor-Induced Vasoconstriction. *Arterioscler Thromb Vasc Biol*. 2018;38:542-554.
5. Liu Y, Terata K, Chai Q, Li H, Kleinman LH and Gutterman DD. Peroxynitrite inhibits Ca2+-activated K+ channel activity in smooth muscle of human coronary arterioles. *Circ Res*. 2002;91:1070-6.
6. Sonkusare SK, Dalsgaard T, Bonev AD, Hill-Eubanks DC, Kotlikoff MI, Scott JD, Santana LF and Nelson MT. AKAP150-dependent cooperative TRPV4 channel gating is central to endothelium-dependent vasodilation and is disrupted in hypertension. *Sci Signal*. 2014;7:ra66.
7. Sonkusare SK, Bonev AD, Ledoux J, Liedtke W, Kotlikoff MI, Heppner TJ, Hill-Eubanks DC and Nelson MT. Elementary Ca2+ signals through endothelial TRPV4 channels regulate vascular function. *Science*. 2012;336:597-601.
8. Chung SH and Kennedy RA. Coupled Markov chain model: characterization of membrane channel currents with multiple conductance sublevels as partially coupled elementary pores. *Math Biosci*. 1996;133:111-37.
9. Navedo MF, Cheng EP, Yuan C, Votaw S, Molkentin JD, Scott JD and Santana LF. Increased coupled gating of L-type Ca2+ channels during hypertension and Timothy syndrome. *Circ Res*. 2010;106:748-56.
10. Seo YH and Carroll KS. Profiling protein thiol oxidation in tumor cells using sulfenic acid-specific antibodies. *Proc Natl Acad Sci U S A*. 2009;106:16163-8.
11. Zielonka J, Sikora A, Joseph J and Kalyanaraman B. Peroxynitrite is the major species formed from different flux ratios of co-generated nitric oxide and superoxide: direct reaction with boronate-based fluorescent probe. *J Biol Chem*. 2010;285:14210-6.
12. Goy C, Czypiorski P, Altschmied J, Jakob S, Rabanter LL, Brewer AC, Ale-Agha N, Dyballa-Rukes N, Shah AM and Haendeler J. The imbalanced redox status in senescent endothelial cells is due to dysregulated Thioredoxin-1 and NADPH oxidase 4. *Exp Gerontol*. 2014;56:45-52.
13. Livak KJ and Schmittgen TD. Analysis of relative gene expression data using real-time quantitative PCR and the 2(-Delta Delta C(T)) Method. *Methods*. 2001;25:402-8.
14. Marziano C, Hong K, Cope EL, Kotlikoff MI, Isakson BE and Sonkusare SK. Nitric Oxide-Dependent Feedback Loop Regulates Transient Receptor Potential Vanilloid 4 (TRPV4) Channel Cooperativity and Endothelial Function in Small Pulmonary Arteries. *J Am Heart Assoc*. 2017;6.
15. Xu Q, Heo CH, Kim G, Lee HW, Kim HM and Yoon J. Development of imidazoline-2-thiones based two-photon fluorescence probes for imaging hypochlorite generation in a co-culture system. *Angew Chem Int Ed Engl*. 2015;54:4890-4.